Published in final edited form as:
Neuroimage. 2013 December ; 83: . doi:10.1016/j.neuroimage.2013.06.042.

Disrupted cortico-cerebellar connectivity in older adults

Jessica A. Bernard[1], **Scott J. Peltier**[2], **Jillian Lee Wiggins**[1], **Susanne M. Jaeggi**[5], **Martin Buschkuehl**[1,5], **Brett W. Fling**[3], **Youngbin Kwak**[4,7], **John Jonides**[1,4], **Christopher S. Monk**[1,4], and **Rachael D. Seidler**[1,3,4,*]

[1]Department of Psychology, University of Michigan

[2]Functional MRI Laboratory, University of Michigan

[3]School of Kinesiology, University of Michigan

[4]Neuroscience Program, University of Michigan

[5]University of Maryland at College Park

[7]Center for Cognitive Neuroscience, Duke University

Abstract

Healthy aging is marked by declines in a variety of cognitive and motor abilities. A better understanding of the aging brain may aid in elucidating the neural substrates of these behavioral effects. Investigations of resting state functional brain connectivity have provided insights into pathology, and to some degree, healthy aging. Given the role of the cerebellum in both motor and cognitive behaviors, as well as its known volumetric declines with age, investigating cerebellar networks may shed light on the neural bases of age-related functional declines. We mapped the resting state networks of the lobules of the right hemisphere and the vermis of the cerebellum in a group of healthy older adults and compared them to those of young adults. We report disrupted cortico-cerebellar resting state network connectivity in older adults. These results remain even when controlling for cerebellar volume, signal-to-noise ratio, and signal-to-fluctuation noise ratio. Specifically, there was consistent disruption of cerebellar connectivity with both the striatum and the medial temporal lobe. Associations between connectivity strength and both sensorimotor and cognitive task performance indicate that cerebellar engagement with the default mode network and striatal pathways is associated with better performance for older adults. These results extend our understanding of the resting state networks of the aging brain to include cortico-cerebellar networks, and indicate that age differences in network connectivity strength are important for behavior.

Keywords

cerebellum; aging; fcMRI; striatum; medial temporal lobe; working memory; sensorimotor performance

*Corresponding Author: Rachael D. Seidler, 401 Washtenaw Avenue, Ann Arbor, MI 48109-2214, Tel: (734) 615-6224, Fax: (734) 936-1925, rseidler@umich.edu.

1. Introduction

Aging is associated with cognitive and motor declines (Park & Reuter-Lorenz, 2009; Seidler et al., 2010). Older adults show declines in cognitive function (Park et al., 2001), and also have deficits in motor learning (Bo et al., 2009; Anguera et al., 2011). Neuroimaging research has demonstrated that older adults show more bilateral patterns of brain activation during both cognitive (Reuter-Lorenz et al., 2000) and motor tasks (Naccarato et al., 2006; Mattay et al., 2002). Furthermore, there are age differences in resting state functional brain networks (Andrews-Hanna et al., 2007; Damoiseaux et al., 2008; Wu et al., 2007; Langan et al., 2010; Wiggins et al., 2011, 2012), along with differences in brain volume (Raz et al., 2005). Investigations of the neural substrates of performance declines with age have focused heavily on the cerebral cortex, despite known age differences in cerebellar volume, and contributions of this structure to both motor and cognitive behaviors (Raz et al., 1998, 2001; Stoodley, et al., 2012; Hoogendam et al., In Press; Bernard & Seidler, In Press). Given the diverse behavioral functions of the cerebellum, along with its known structural differences in young and older adults, further investigation in aging, particularly with respect to resting state networks, is warranted.

Resting state functional connectivity MRI analyses have provided insight into the networks of the aging brain. The default mode network (DMN) has been especially well studied (Andrews-Hanna et al., 2007; Damoiseaux et al., 2008). Connectivity within the DMN is decreased in older adults and is related to performance on cognitive tasks (Andrews-Hanna et al., 2007; Damoiseaux et al., 2008). There are also age differences in functional motor cortical connectivity, which are associated with motor performance (Wu et al., 2007; Langan et al., 2010). While these studies indicate that there are age differences in cortical resting state brain networks, none has investigated cerebellar connectivity. Investigating resting state cortico-cerebellar networks may provide key insight into both the motor and cognitive declines associated with healthy aging.

The cerebellum plays a role in a wide variety of motor and cognitive behaviors, and the structure contains a well-defined functional topography (Stoodley & Schmahmann, 2009; Stoodley et al., 2012). Anterior lobules and lobules VIIIa and VIIIb are associated with motor functions, whereas the remaining posterior lobules are associated with cognitive functions. Furthermore, there are connections between anterior regions of the cerebellum (specifically, lobules IV and V) as well as lobule VIII in the posterior cerebellum with the motor cortex, and separate loops connecting the lateral and posterior cerebellum (particularly Crus I and Crus II) and the prefrontal cortex (Middleton & Strick, 2001; Kelly & Strick, 2003; for a review see Strick et al., 2009). Converging evidence for dissociable structural connections has also been found in the human brain (Salmi et al., 2009). Resting state cortico-cerebellar networks have been extensively mapped in young adults (Buckner et al., 2011; Krienen & Buckner, 2010; O'Reilly et al., 2010; Habas et al., 2009; Bernard et al., 2012; Bernard et al., In Press). However, a gap in the literature exists with respect to age differences in cortico-cerebellar network connectivity. Quantifying these age differences may provide key insights into age declines in motor and cognitive function. Given the functional topography within the cerebellum, and its roles in both motor and cognitive task performance, it is a potentially important target of investigation in aging.

In the current study we used resting state functional connectivity magnetic resonance imaging to map large-scale cortico-cerebellar networks in older adults. We compared these results with maps previously reported for young adults (Bernard et al., 2012), while controlling for the potentially confounding influences of signal-to-noise ratio (D'Esposito et al., 2003) and cerebellar volume. Given the indication of decreased resting state connectivity in older adults' cortical networks (Andrews-Hanna et al., 2007; Wu et al., 2007;

Damoiseaux et al., 2008), we hypothesized that cortico-cerebellar connectivity would also be decreased in older adults. A subset of older adult participants completed a sensorimotor and cognitive test battery, allowing us to investigate the relationships between cortico-cerebellar network connectivity strength and behavior. We predicted that connectivity strength of lobules in the anterior cerebellum would be associated with sensorimotor task performance, while connectivity strength of posterior lobules (excluding lobules VIIIa and VIIIb which are associated with motor functions), particularly Crus I and Crus II would be associated with cognitive behaviors.

2. Method

2.1 Participants

We recruited 35 older (age ± stdev; 64.55 ± 6 years, 13 females) and 38 young adults (22.76 ± 2.95 years, 17 females) from the University of Michigan and greater Ann Arbor community as part of a larger study. All participants were healthy, with no history of neurological or psychiatric disorder, and had no contraindications for fMRI scanning. Participants signed a consent form approved by the University of Michigan Medical Institutional Review Board. Three young adult participants were excluded from analyses due to motion artifacts, and two young adult participants were excluded due to technical problems during data collection, leaving a total of 33 (15 female) young adult participants. Data from the young adults have been previously reported (Bernard et al., 2012) and serve as an age comparison group for the older adults in this study.

2.2 fMRI Data Acquisition

Functional MRI data were collected with a 3T GE Signa scanner at the University of Michigan. A single-shot gradient-echo reverse spiral pulse sequence (Glover and Law, 2001) was used to collect either 300 (all older adults and n=12 young adult participants) or 240 (n = 18 young adult participants) T2*-weighted BOLD images (TR=2s, TE=30 ms, flip angle = 90°, FOV = 220 mm × 220mm, voxel size = 3.4 mm × 3.4 mm × 3.2 mm, 40 axial slices). For the structural images, a 3D T1 axial overlay (TR=8.9 ms, TE= 1.8 ms, flip angle= 15°, FOV= 260 mm, slice thickness = 1.4 mm, 124 slices; matrix = 256 × 160) was acquired for anatomical localization. To facilitate normalization, a 110-slice (sagittal) inversion-prepped T1-weighted anatomical image using spoiled gradient-recalled acquisition in steady state (SPGR) imaging (flip angle = 15°, FOV = 260 mm, 1.4 mm slice thickness) was acquired. A visual fixation cross was presented to the subject using a rear projection visual display. Participants were instructed to look at the cross and not to think about anything in particular. A pressure belt was placed on the abdomen of each subject to monitor the respiratory signal. A pulse oximeter was placed on the subject's finger to monitor the cardiac signal. The respiratory, cardiac, and fMRI data collection were synchronized such that the onset of the resting state scan was time-locked with the onset of collection of both the cardiac and respiratory signals.

2.3 fMRI Data Analysis

The functional MRI data were preprocessed as part of the standard processing stream at the University of Michigan. First, K-space outliers in the raw data greater than two standard deviations from their mean were replaced with the average of their temporal neighbors. Second, images were reconstructed using field map correction to remove distortions from magnetic field inhomogeneity. Third, physiological variations in the data from the cardiac and respiratory rhythms were removed via regression (Glover et al., 2000). This removed the effects of the first and second order harmonics of the externally collected physiological waveforms. Fourth, slice-timing differences were corrected using local sinc interpolation (Oppenheim et al., 1999). Lastly, we used MCFLIRT in the fMRIB Software Library

(Jenkinson et al., 2002) to perform motion correction (using the 10th image volume as the reference). For all participants, head motion was less than 0.1 mm in the x, y, or z direction (young adult average = 0.09, 0.03, and 0.02 mm and older adult average=.006, .004, and .003 mm, in the x, y, and z directions, respectively). Structural images were skull-stripped using FSL and we then registered the 3D T1 SPGR to the functional images using Advanced Normalization Tools (ANTS; Avants, et al., 2008; Penn Image Computing & Science Lab, http://www.picsl.upenn.edu/ANTS/). The data were then normalized to MNI space using ANTS. Additionally, because of the potential for distortions when normalizing the cerebellum to standard space (Diedrichsen et al., 2009), the cerebellum was normalized separately to a spatially unbiased atlas template (SUIT; Diedrichsen, 2006; Diedrichsen et al., 2009) also using ANTS. This resulted in normalized whole-brain structural and functional images, and separately normalized cerebellar structural and functional images.

2.4 Functional Connectivity Analysis

Because of the variable duration of the resting state scans, only the *first* 8 minutes of functional data were used in our analyses. Additionally, the first five volumes were discarded to all for scanner equilibration. The following procedures were used to generate functional connectivity maps (low frequency time course correlation maps). The data were first filtered using a second order dual-pass band-pass filter to examine the band of interest (0–0.08 Hz) and to exclude higher frequency sources of noise such as heart rate and respiration (Biswal et al., 1995; Peltier et al. 2003).

Second, the time course of BOLD activity was extracted from each of the 10 lobules within the right cerebellar hemisphere and 8 lobules within the vermis using masks created with the SUIT atlas (Diedrichsen et al., 2009). The SUIT atlas and normalization method was developed to more accurately investigate the cerebellum, and used anatomical landmarks to validate the normalization and lobular regions (Diedrichsen, 2006; Diedrichsen et al., 2009). These 18 lobules were used as the seed regions in our resting state analysis. Because very little is known about the cerebellum in aging, we chose to investigate all of these lobules, though we limited our investigation to the dominant (right) hemisphere. This created an average timecourse for all of the voxels within the mask. For individual lobules that were not fully included in the mask due to coverage of the cerebellum in a particular participant, these individuals were not included in the analysis for that particular lobule. The resultant sample size is indicated with the results. Notably, Lobules I, II, III, and IV are combined in the SUIT atlas so they were investigated together. They are henceforth referred to as Lobules I–IV. Furthermore, it is notable that lobules I–III have minimal connections with motor cortical regions (Kelly & Strick, 2003), but given their small size and the limitations of the SUIT atlas, we were unable to investigate them separately. We were also unable to successfully create a mask for Vermis Crus I, and were therefore unable to include this lobule in our analyses. Third, the timecourse of the seed region was unit normalized to remove differences in mean and variance between spatial regions. Fourth, the average seed region timecourse in the filtered data was correlated with all other low-pass filtered voxels in both the cerebellum and the whole brain functional data (done in two separate steps on smoothed functional data) to form functional connectivity maps for each region of interest in each participant. The connectivity maps were converted to z-scores using Fisher's r-to-z transform. Z scores from each participant were entered into the group-level analyses, which were carried out using SPM5 (Wellcome Department of Cognitive Neurology, London, UK; http://www.fil.ion.ucl.ac.uk). The group level-analyses for the younger adults were previously reported (Bernard et al., 2012), so we only present the group-level analyses for the older adults. We evaluated the connectivity maps associated with each lobule individually using a family-wise error correction of $p<0.005$ (unless otherwise indicated) with a voxel extent threshold of at least 100 voxels (Nichols & Hayasaka, 2003). Finally,

group comparisons for the young and older adults were conducted in SPM5 using two-sample t-tests for each lobule of the right hemisphere and the vermis. Because so little is known about cortico-cerebellar networks in older adults, we evaluated the age differences using an uncorrected $p<.001$, with a voxel extent threshold of at least 10 voxels, comparable with what was used in previous work comparing resting state connectivity across groups (Kwak et al., 2010). This more lenient threshold allowed us to get a wider picture of the age differences in these networks.

2.4.1 Control Analyses—We completed follow-up analyses to control for the following potential confounding factors in the age group comparisons: whole-brain signal-to-noise ratio (SNR), whole brain signal-to-fluctuation-noise ratio (SfNR), and lobular volume. SfNR has been argued to be more important for fMRI studies, as it encompasses change in the relative signal over time (Schmiedeskamp et al., 2010). SNR and SfNR were calculated based on equations from Schmiedeskamp and colleagues (2010). SNR was calculated by taking the average time course across the whole brain, and dividing it by the standard deviation (stdev):

$$SNR = mean(whole\ brain\ functional\ image) / stdev(whole\ brain\ functional\ image)$$

SfNR was calculated for each individual voxel, by dividing the average signal of each voxel over the timecourse by its standard deviation over time:

$$SfNR = (1/n * \sum S(t)) / \sigma_t$$

S(t) is the signal in an individual voxel over time, σ_t is the standard deviation of the signal over time, and n is the number of timepoints. The average over all the voxels was taken to produce a single value indicative of the standard deviation of the signal over time. The SNR and SfNR calculations were completed on spatially unsmoothed and temporally unfiltered data.

Finally, we also calculated the volume for each lobule in the right hemisphere and the vermis. The cerebellum was first extracted from the high-resolution (SPGR) anatomical images using the SUIT toolbox (Diedrichsen, 2006; Diedrichsen, et al., 2009). This resulted in a structural image of the isolated cerebellum, along with probability maps indicating the probability of each voxel in the volume belonging to the cerebellum and brainstem. We masked our structural images with the probability maps, yielding a structural image of the cerebellum and brainstem only, excluding any surrounding cortical tissue.

Next, we used the lobular regions described in the SUIT atlas (Diedrichsen, 2006; Diedrichsen et al., 2009) to determine individual lobular volumes of each subject for all lobules in the right hemisphere and the vermis. First, we created masks of each lobule using the probabilistic SUIT atlas. This resulted in 17 masks (Figure 1). Second, the SUIT cerebellum template was normalized to each individual subject's cerebellar anatomical image (in native space) using ANTS. The transformation was first applied to the SUIT cerebellum, and then the resulting warp vectors were applied to the individual lobular masks. The result was a mask of each lobule normalized to individual subject space for each participant.

Finally, these masks were loaded into MRICron (http://www.mccauslandcenter.sc.edu/mricro/mricron/index.html) and converted to volumes of interest. They were overlaid onto each individual subject's structural scan and inspected to ensure accurate registration. We

then used MRICron to calculate the descriptive statistics for each lobule, providing us with the gray matter volume of each lobule in cubic centimeters. This procedure was repeated for each participant.

Additionally, we calculated the total intracranial volume (TIV) for all participants to normalize the cerebellar lobular volumes. We first segmented the gray matter, white matter, and cerebrospinal fluid using the segment function in SPM5. The SPM5 VBM toolbox was used to get the total volume for each of these tissue types, in each individual subject, in native space. The volume of the gray matter, white matter, and cerebrospinal fluid were summed to get the TIV for each individual. Normalized lobular volumes were calculated by dividing the total lobular volume by the TIV. These normalized values were used in our control analyses.

Age differences in SNR and SfNR were evaluated using independent samples t-tests. Age differences in lobular volume were evaluated using a 2×17 age by lobule repeated measures ANOVA. Follow-up t-tests were performed to investigate age differences in individual lobules. These t-tests were interpreted using a Bonferroni correction with an alpha of .003. To investigate the effects of SNR, SfNR, and lobular volume, we ran multiple regression analyses in SPM5 on lobules where the young adults showed significantly greater resting state connectivity than the older adults. All of the older adult time courses for a particular lobule were entered into the regression, along with SNR, SfNR, and lobular volume. The analyses were masked with the appropriate young greater than older adults contrast. This allowed us to investigate whether resting state connectivity declines in the older adults were associated with the potential confounding influences of SNR, SfNR, and regional cerebellar volume. The results of these analyses were investigated using an uncorrected threshold of $p<.001$ with a minimum cluster size of 10 voxels. This threshold matched what was used in the age contrasts.

2.5 Behavioral Assessment

Our older adult participants were invited to return to the lab for a second day of behavioral testing. A total of 14 individuals from this sample (average age, 62.9 ± 7.4 years, 3 females) returned to complete the assessments.

2.5.1 General Cognitive Function and Task Switching—General cognitive function was measured using the Montreal Cognitive Assesment (MOCA; Nasreddine et al., al 2005) and task switching was measured with the Trail-making task (A and B versions; Reitan et al., 1985). The Trails A task is indicative of visual attention, while the Trails B task measures task switching and executive control. We recorded the time to complete the A and B portions of the Trail-making task, along with the difference between the two conditions (B-A, measured in seconds). We used the difference score in our analyses, to assess relationships with control and task switching, above and beyond visual attention.

2.5.2 Working Memory—We administered a verbal working memory Sternberg task (Sternberg, 1966) similar to that used by Desmond and colleagues (2005) using E-Prime 2.0 software (Psychology Software Tools, Inc). Four lowercase letters were presented in white, size 20 Courier New font on a black background around a centrally located fixation cross for 1500 msec. This was followed by a 3000-msec retention interval after which a capitalized letter was presented for 1500 msec. During the presentation of this letter, participants were asked to make a yes or no button press response to indicate whether or not the letter was a part of the previously viewed set. There was an additional 1500 msec after the presentation of the capitalized letter during which participants could make their response. This resulted in a total inter-trial interval of 7500 msec. Participants completed 144 trials (3 blocks of 48

trials each). We recorded accuracy (% correct) along with reaction time (msec) on correct trials for all participants.

2.5.3 Visuomotor Adaptation and Choice Reaction Time—A visuomotor adaptation task was administered using Presentation 14.5 software (Neurobehavioral Systems, Albany, CA) on a desktop computer (Imamizu et al., 2000; Inoue et al., 2000; Anguera et al., 2009). Targets (0.8 cm in diameter) were presented for 4 seconds in one of four locations: 4.8 cm to the right, left, above, or below a central starting position (0.8 cm in diameter). Participants controlled a cursor using their whole hand to move a standard gaming joystick (Logitech Extreme 3D joystick, Fremont, CA) placed on the desk in front of them. They were asked to move the cursor to the target circle as quickly and as accurately as possible and to maintain the cursor in the target circle until it disappeared. Upon disappearance of the target, participants were asked to release the joystick so the cursor would re-center itself. The next trial began 1 second later, resulting in a total inter-stimulus interval of 5 seconds. Participants performed 14 blocks of the task (24 trials per block), with the first two experimental blocks under veridical feedback conditions. This was followed by 10 adaptation blocks with visual feedback rotated 30° clockwise about the center of the screen, and finally two more blocks again under veridical feedback conditions.

The x and y coordinates from the joystick were recorded at a rate of 100 Hz. The data were analyzed offline using custom MATLAB (MathWorks, Inc, Natick, MA) programs. The data were first filtered with a dual low-pass Butterworth digital filter, using a cutoff frequency of 10 Hz, and then the resultant joystick path was calculated (square root of the sum of the squared x and y coordinates at each time point). The tangential velocity profile was then calculated through differentiation of the resultant position data. Movement onset and offset were computed through the application of Teasdale, Bard, Fleury, Young, and Proteau's (1993) optimal algorithm to the velocity profile for each movement. Learning was assessed by measuring direction error (DE), which is the angle between a straight line from the start to the target position and a straight line from the start to the actual position attained at the time of peak velocity. We assessed performance during the adaptation and washout periods by fitting exponential functions to the trial-by-trial data (cf. Benson et al., 2011). These fits resulted in an intercept and decay constant that characterized the adaptation and washout performance. In our subsequent analyses we used the decay constant to describe adaptation and the intercept to model washout. The first block of testing under veridical feedback served as a practice block. The second block of testing, still under veridical feedback, allowed us to measure choice reaction time. Here, we measured reaction time to move to the target (average over all trials).

2.5.4 Timing—Timing was measured using a synchronization-continuation tapping task (Wing & Kristofferson, 1973) administered with E-Prime 2.0 software (Psychology Software Tools, Inc). Participants sat comfortably in front of the computer screen with their gaze centered on a fixation cross, and they were instructed to press the "z" key on the keyboard in synchrony with a periodic auditory tone. Each trial began with the message "ready, go" presented on the computer screen, followed by the presentation of the periodic tone. Participants were instructed to listen to the tone and to synchronize their taps with the tone. After their initial response, twelve additional beats were presented while the participant tapped along. Following the twelve beats, the tone was removed and participants were asked to keep tapping to that beat as consistently as possible. The trial ended after 30 un-paced beats. There were three interval conditions: 500, 1000, and 1500 ms. Participants completed 5 trials of each of the three interval conditions with each hand (15 trials per hand), as well as practice trials prior to the start of each block. The order of hands was counterbalanced across participants.

Timing was quantified using the coefficient of variance (CV). The coefficient of variance is calculated by dividing the standard deviation of the inter-tap-interval by the mean duration of the inter-tap-interval. The mean CV for each hand and time interval was calculated. Analyses focused on the CV for the un-paced continuation phase (30 taps without the tone) completed using the dominant (right) hand. All three interval conditions were analyzed.

2.5.5 Balance—We assessed balance using the activities-specific balance confidence (ABC) scale (Powell et al., 1995) and with a one-legged timed standing balance task. The ABC scale asks participants to rate their confidence (from 0–100% confident) in performing 16 everyday tasks, including walking up and down stairs, walking on icy sidewalks, and walking across a parking lot. For the one-legged standing balance task participants stood on their dominant (right) leg with their arms crossed over their chest. They were timed (maximum of 90 seconds) from the point of taking their foot off the ground until it was placed back on the ground. A research assistant spotted the participants from behind throughout this process. Trials with eyes opened and closed were completed (three trials per condition).

2.5.6 Manual Dexterity—To assess manual dexterity, we used the grooved pegboard (Lafayatte Instruments, Lafayette, IN). We quantified the time it took participants to fill all of the holes with “T” shaped pegs. This was completed with the dominant (right) hand.

2.5.7 Correlations with Resting state Networks—We investigated whether cortico-cerebellar connectivity strength predicts behavioral performance in older adults. Behavioral performance was used in correlation analyses with cortico-cerebellar connectivity, completed in SPM5. The functional networks for each older adult individual were entered into the analysis and task performance was entered as a covariate (each task was entered individually). All analyses were masked with the whole brain older adult resting state network for the lobule in question. We evaluated the correlations within these masks using an uncorrected $p<.001$, with a voxel extent threshold of at least 10 voxels. We looked at positive correlations for balance confidence, standing balance time (eyes opened and closed), general cognitive function (MOCA), working memory accuracy, and visuomotor adaptation. Reaction time measures and variability in timing performance were evaluated with negative correlations, as smaller values on these tasks indicate better performance. We were unable to investigate the networks of lobules VIIIa and VIIIb. Only a subset of our participants returned for behavioral testing, and these lobules were often excluded due to lack of sufficient coverage. Once these two factors were both taken into account, the sample size of those with both behavior and sufficient coverage of these lobules was too small ($n=5$).

3. Results

3.1 Older Adult Lobular Networks

We have previously reported the resting state cortico-cerebellar networks for young adults (Bernard et al., 2012). Here we report only the networks in the older adults, and age differences in the networks. We present areas of correlation within the cerebellum separately from those in the cortex because of our normalization procedures. However, we speculate that these correlations in the cerebellum may be reflective of a cortical region driving the correlation, rather than intracerebellar correlations across lobules. Connections across cerebellar regions are minimal, and distinct regions of the cerebellum are associated with dissociable closed-loop circuits with the cortex (Strick et al., 2009). Given these anatomical constraints, it is likely that cerebellar regions showing connectivity in the resting state have correlated cortical targets as part of their respective cortico-cerebellar circuits. Areas of

correlation within the cerebellum were identified using the spatially unbiased atlas of the cerebellum (Diedrichsen, 2006; Diedrichsen et al., 2009). Regions of correlation in the medial motor areas were localized using the atlas provided in Picard and Strick (1996). The general patterns of the results are described below. For complete lists of correlated regions within the cerebellum and the cortex, as well as the sample size included in each analysis, please see Tables 1 and 2. Table 1 presents the correlations between the lobules of the right hemisphere and the vermis within the cerebellum, while Table 2 presents the correlations with the whole brain.

Within the cerebellum, all of the lobules were strongly correlated with themselves. Given that we used an average timecourse in our analyses, and we ran our correlation with every individual voxel within the brain, this is to be expected. Overall, the resting state networks of the older adults display patterns quite similar to those we previously described in young adults (Bernard et al., 2012). Lobules I–IV, V and VI were strongly correlated with themselves as well as Lobule VIIIa, which is also implicated in motor networks (Krienen & Buckner, 2009; Kelly & Strick, 2003). The posterior lobules, with the exclusion of lobules VIIIa and VIIIb (which were only significantly self-correlated) were primarily correlated with other posterior lobules. However, it is notable that in both the anterior and posterior regions of the cerebellum there were also correlations with lobules across the general anterior-posterior divide.

In the cortex, however, the patterns in the older adults deviate from what we found in the young adults (Bernard et al., 2012). In the young adults, lobules I–IV, V, and VI are part of cortico-cerebellar networks involving pre-motor and primary motor cortical regions. However, in the older adults, the correlations were more widespread, including the hippocampus, middle frontal gyrus, parrahippocampal gyrus, anterior cingulate cortex, and the dorsal pre-motor cortex. The only correlations with the primary motor cortex were with lobule VI. Lobules VIIIa and VIIIb did not show any correlations with motor cortical regions; although this is consistent with our findings in young adults, it is nevertheless somewhat unexpected. The remaining posterior lobules were correlated with prefrontal cortex, as well as the caudate, thalamus, and temporal cortex regions. The lobules of the vermis had comparable diffuse networks that included primarily prefrontal and parietal cortical regions. However, in the older adults there were no correlations with the primary motor and pre-motor cortical regions, unlike our findings in young adults (Bernard et al., 2012). Finally, there were no significant whole-brain correlations for right hemisphere lobules VIIb and X, nor for vermis Crus II, VIIb, or X.

3.2 Age Differences in Cortico-Cerebellar Networks

We compared connectivity patterns in the young relative to the older adults. We contrasted the networks of the two age groups to test for areas with greater connectivity in young adults, as well as areas with greater connectivity in older adults. We present general findings below. The specific regions of correlation as well as the sample sizes used in each contrast are presented in Tables 3–8. Tables 3–6 present the results of the young greater than older adults contrast, while Tables 7 and 8 present the results from the older greater than young adults contrast.

For the young greater than older adult contrast several interesting patterns emerged. There is an overall decrease in the strength of large-scale resting state cortico-cerebellar networks in the older adults, evidenced by the widespread regions of greater connectivity in the young adults consistent with the previously mapped young adult netwoks (Bernard et al., 2012).

In the whole brain, most striking was the greater connectivity between the cerebellum and the striatum in young versus older adults. This pattern was consistent across multiple large-

scale cortico-cerebellar networks (Figures 2–4). The majority of lobular networks had greater striatal-cerebellar connectivity in the young adults. Additionally, our analyses revealed greater connectivity between lobules in both the right hemisphere and the vermis with the hippocampus and the parahippocampal gyrus in the medial temporal lobe. Finally, the greater connectivity in the young adults was generally restricted to non-motor areas, regardless of the lobular network, with the exception of several correlations with pre motor and cingulate motor regions.

The majority of networks also had regions of connectivity that were greater in older than young adults (Tables 7 and 8). However, these regions were generally quite sparse and small in area. Within the cerebellum, across multiple lobular networks these regions were primarily in lobules VIIIa and VIIIb. In the cerebral cortex, across multiple networks there were stronger correlations in the inferior frontal gyrus, as well as temporal and parietal regions. Interestingly, these regions of greater connectivity in older adults were with pre-frontal cortical areas, even for lobular seeds that are more typically associated with motor functions. This was particularly notable for lobule VIIIb which showed greater connectivity with pre-frontal, temporal, and partietal regions in older adults. Overall, these regions of greater connectivity in the older adults are outside of the lobular networks as mapped in both young and older adult analyses, perhaps indicative of some form of compensation for the overall decreased cortico-cerebellar connectivity seen here in aging.

3.3 Control Analyses

We first compared whole brain SNR, SfNR, and normalized lobular volumes between young and older adults. The average SNR was 67.06 (± stdev, 13.22) in the young adults and 67.32 (±3.5) in the older adults. The average SfNR was 75.56 (±24.86) in the young adults and 73.45 (±24.08) in the older adults. There were no significant age differences in SNR ($t_{(68)}$= −.112, p=.91) nor in SfNR (($t_{(70)}$=.365, p=.72). With respect to lobular volume, there were significant main effects of age ($F_{(1,49)}$=18.25, p<.001) and lobule ($F_{(3.06, 149.93)}$=2004.09, p<.001) and a significant age by lobule interaction ($F_{(3.06, 149.93)}$=6.640, p<.001). A Greenhouse-Geisser correction was used to account for violations of sphericity. Follow-up t-tests, corrected for multiple comparisons, indicated significant age differences in lobules I–IV ($t_{(50)}$=4.91, p<.001), lobule V ($t_{(50)}$=4.06, p<.001), lobule VI ($t_{(50)}$=5.61, p<.001), Crus II ($t_{(50)}$=3.21, p<.003), vermis lobule VI ($t_{(50)}$=5.86, p<.001), and vermis lobule VIIb ($t_{(49)}$=4.11, p<.001), with smaller volumes for older than young adults.

The results of our control analyses revealed several small correlations between our covariates and connectivity strength in areas that show stronger connectivity in young adults than older adults. Please see Table 9 for a complete listing of these regions. Importantly, these correlations were only seen for two networks (those of lobules V and VI), and were limited to the cerebellum, posterior cingulate cortex, and precuneus. Thus, the majority of the results of our young greater than older adults age contrast are not due to these potentially confounding factors.

We also investigated age differences in movement in the X, Y, and Z directions during the scanning session. Our results indicated a significant main effect of age ($F_{(1,76)}$=17.54, p<.001), such that younger adults had *more* head movement than older adults. However, in both age groups this movement was minimal (range across all directions: young adults =.02–.09 mm, older adults = .003–.006 mm).

3.4 Network Connectivity and Behavior

Finally, we investigated correlations between sensorimotor and cognitive task performance with resting state cortico-cerebellar network connectivity strength in older adults. We have

previously reported age differences in task performance in this sample (Bernard & Seidler, In Press). Across the majority of the tasks investigated, older adults showed impaired performance, though there was no difference in the MOCA score, indicating the general overall cognitive health of our sample, and older adults performed better on the timing task than young adults. The results of our analyses relating connectivity strength to behavior are listed in Table 10; they revealed two interesting patterns. However, given the small sample size used in our analyses, and that these analyses were completed using an uncorrected p-value, they should be interpreted with caution. First, correlations between multiple lobules of the cerebellum and both the caudate and thalamus were predictive of behavior (Figure 5a). This is particularly notable given the age differences in connectivity between cortico-cerebellar networks and the striatum. Second, resting state connectivity strength between Crus II and the posterior cingulate cortex or precuneus was correlated with measures of balance, timing, manual dexterity, and working memory (Figure 5b). In all cases, stronger connectivity was associated with better performance. However, in cases where reaction time was the primary outcome measure, and timing where lower variability indicates better performance, strong negative correlations were seen (i.e. greater connectivity strength was associated with shorter reaction times and reduced temporal variability).

4. Discussion

The goal of this study was to examine age differences in cortico-cerebellar network connectivity. Consistent with our hypothesis, we observed widespread decreases in resting state connectivity of older adults across the lobular networks we investigated. However, there were no differential patterns by functional cerebellar regions (i.e. “motor” versus “cognitive” lobules). This indicates that cortico-cerebellar networks, regardless of functional type, are equally impacted by aging. Several interesting patterns emerged within the results. Across multiple networks, aging disrupted the interactions between cortico-cerebellar networks and the striatum. This was evidenced by greater connectivity between the cerebellar lobules and the striatum in young adults. We also report similar disruptions in the networks of the cerebellar lobules and medial temporal lobe regions, including the hippocampus. Importantly, these age differences were not associated with the potentially confounding factors of SNR, SfNR, and cerebellar lobular volume. The only exceptions to this were in small areas of the cerebellum, and the greater connectivity between lobule VI and the posterior cingulate cortex in young adults. These patterns and their potential implications are discussed in turn below.

Across numerous lobules, we observed a pattern indicative of disrupted connectivity between large-scale cortico-cerebellar networks and the striatum. Consistently, young adults showed stronger connectivity between cerebellar regions and both the caudate and putamen. Bidirectional anatomical connections between the cerebellum and the striatum have been mapped in the non-human primate (Hoshi et al., 2005; Bostan et al., 2010). We have also demonstrated resting state correlations between the cerebellar lobules and the striatum in young adults (Bernard et al., 2012). Furthermore, both the cerebellum and basal ganglia are part of a network important for motor task switching, though older adults are known to engage these regions to a lesser extent than young adults (Coxon et al., 2010). We speculate that disrupted connectivity between the cerebellum and basal ganglia in older adults may be due to age declines in dopamine levels.

There are decreases in dopamine with healthy aging, particularly in the substantia nigra (Fearnley & Lees, 1997; McGeer et al., 1977). We speculate that dopaminergic declines may have contributed to the decreased striatal-cerebellar connectivity observed in the older adults. Indeed, increasing dopamine levels in healthy young adults with l-dopa increased connectivity in motor pathways between the putamen and the cerebellum (Kelly et al.,

2009). Natural decreases in dopamine may then decrease connectivity in these pathways. This further underscores the importance of investigating these networks in Parkinson's disease given the hallmark dopaminergic depletion. As Hoshi et al. (2005) speculated, alterations in the networks connecting these two regions may relate to disease symptomatology. However, further research is needed to investigate this hypothesis directly, as our results do not rule out other possibilities. Indeed, the presence of amyloid plaques has been shown to disrupt connectivity of the default mode network in healthy aging (Sheline et al., 2010). Though we are looking at cortico-cerebellar networks, a similar mechanism may be at play here, and could only be ruled out with further investigation.

The second striking pattern that we observed was reduced connectivity between large-scale cerebellar networks and the medial temporal lobe in older adults. Connectivity with the hippocampus was particularly impacted. Young adults consistently showed greater connectivity with medial temporal lobe regions across multiple networks. This is particularly pertinent given that investigations of Alzheimer's disease and amnestic mild cognitive impairment have revealed decreased connectivity between the cerebellum and hippocampus, relative to age matched controls (Allen et al., 2007; Bai et al., 2009). Studies using animal models have suggested that there are direct anatomical connections between the fastigial nucleus of the cerebellum and the hippocampus (Heath & Harper, 1974). This may provide a neural substrate for these resting state correlations. Importantly, it may be that disrupted connectivity between the cerebellum and hippocampus in healthy aging underlies, in part, the deficits in memory and associative learning seen in healthy aging (Craik, 1995; Maguire & Frith, 2003; Woodruff-Pak et al., 2001). However, future research is required, to investigate this more directly.

The majority of our results have focused on age-related disruptions in large-scale cortico-cerebellar networks. However, some networks showed areas of correlation that were greater in older relative to young adults. These areas of correlation were often outside the lobular networks mapped in both age groups. Interestingly, these correlations often included prefrontal areas for predominantly motor networks (as is the case for lobule V and VIIIb). It is possible that these regions are recruited in compensation for the overall decrease in cortico-cerebellar connectivity in older adults. However, we did not see any direct correlations between the behaviors we investigated and these areas. With respect to motor performance however, it is notable that older adults often engage additional cognitive regions in addition to motor regions (Heuninckx et al., 2005; Heuninckx et al., 2008; for a review see Seidler et al., 2010). If we consider that resting state connectivity is perhaps indicative of coactivation during task performance, areas of increased correlation between motor lobules and more cognitive cortical regions are not surprising in older adults given their increased reliance on cognitive resources for motor performance. More generally, these areas of increased connectivity in older adults further support age-related alterations in resting state cortico-cerebellar dynamics.

The influence of head motion on functional connectivity is a potential concern when comparing groups that may differ in head motion (Van Dijk et al., 2012). Here, the young adults exhibited significantly greater head motion than the older adults. When considering this within the context of the impact of head motion on resting state networks (Van Dijk et al., 2012) it is unlikely that this age difference has a significant effect on our results. Increased head motion is associated with *weaker* functional connectivity in large-scale networks such as the DMN, though it is also associated with stronger local connectivity (Van Dijk et al., 2012). In this study we were investigating large-scale networks. We would expect that the impact of head motion would be more pronounced in young adults, weakening the cortico-cerebellar networks of interest. If anything, it may be that there are

greater age differences in the cortico-cerebellar networks in this sample. Notably, in both groups head motion was relatively minimal.

We observed significant relationships between resting state connectivity strength of Crus II and the posterior cingulate with multiple sensorimotor and cognitive behaviors. Crus II has been implicated as playing a role in the DMN (Buckner et al., 2011; Bernard et al., 2012). The posterior cingulate cortex (Greicius et al., 2003) is also a key node in this network. It may be that cerebellar engagement with the DMN is important for understanding behavioral variability in older adults. This is consistent with data indicating correlations between DMN connectivity and behavior in older adults (Andrews-Hanna et al., 2007). We speculate that tighter coupling between nodes of the DMN may result in more efficient task-related deactivation of the network, resulting in better task performance.

Connectivity between lobular networks of the cerebellum and the caudate nucleus were also frequently associated with function. For example, connectivity between Crus II and the caudate nucleus was associated with balance performance. Connectivity between vermis VIIIa and the caudate nucleus was associated with both timing performance and manual dexterity. These correlations are notable given the disrupted connectivity between the cerebellum and the striatum in older adults. Notably, the mechanisms underlying these correlations are unclear, but they highlight the interactions between the cerebellum and basal ganglia for motor performance. Again, stronger coupling between these two brain regions results in better performance, perhaps because the cerebellum can more effectively communicate signals regarding ongoing performance to the basal ganglia allowing for more effective motor control. Though these correlations were small, and in all cases should be interpreted with caution due to our small sample size, they highlight the importance of investigating the behavioral impact of striatal-cerebellar connectivity in cases of pathology.

This work has raised many new empirical questions related to the underlying causes and impact on behavior of age differences in network connectivity strength (e.g. are differences due to decreases in dopamine, the presence of amyloid plaques, an interaction between these factors, or other variables that remain unknown at this time). Future more targeted work will be necessary to gain a full understanding of cortico-cerebellar networks in the aging brain, which may in turn provide us with further insight into the role of the cerebellum in both motor and cognitive aging.

5. Conclusions

We demonstrated that large-scale resting state cortico-cerebellar networks are disrupted in older adults. Most notably, these disruptions were between cortico-cerebellar networks and the striatum, and the hippocampus. These age differences have potential implications for understanding age-related behavioral declines in both sensorimotor and cognitive function. They also may improve our understanding of both Parkinson’s and Alzheimer’s diseases. Finally, we demonstrated that cerebellar contributions to the DMN, and striatal-cerebellar connectivity, were both associated with sensorimotor and cognitive performance in older adults.

Acknowledgments

J.A.B. was supported by NIA T32 AG000114 (S. Pletcher, PI). J.A.B. and R.D.S are members of the International Max Planck Research School on the Life Course (LIFE; www.imprs-life.mpg.de; indcluding: MPI for Human Development, Humboldt-Universität zu Berlin, Freie Universität Berlin, University of Michigan, University of Virginia, University of Zurich). Thanks to K. Hassevoort, M. Lawson, L. Wu, & M. Smith for helping with data processing and analysis.

References

Allen G, Barnard H, McColl R, Hester AL, Fields JA, Weiner MF, Cullum CM. Reduced hippocampal functional connectivity in Alzheimer disease. Archives of Neurology. 2007; 64:1482–1487. [PubMed: 17923631]

Andrews-Hanna JR, Snyder AZ, Vincent JL, Lustig C, Head D, Raichle ME, Buckner RL. Disruption of large-scale brain systems in advanced aging. Neuron. 2007; 56:924–935. [PubMed: 18054866]

Anguera JA, Reuter-Lorenz PA, Willingham DT, Seidler RD. Contributions of spatial working memory to visuomotor learning. Journal of Cognitive Neuroscience. 2009; 22:1917–1930. [PubMed: 19803691]

Anguera JA, Reuter-Lorenz PA, Willingham DT, Seidler RD. Failure to engage spatial working memory contributes to age-related declines in visuomotor learning. Journal of Cognitive Neuroscience. 2011; 22:1917–1930. [PubMed: 19803691]

Avants BB, Epstein CL, Grossman M, Gee JC. Symmetric diffeomorphic image registration with cross-correlation: evaluating automated labeling of elderly and nerodegenerative brain. Medical Image Analysis. 2008; 12:26–41. [PubMed: 17659998]

Bai F, Zhang Z, Watson DR, Yu H, Shi Y, Yuan Y, Qian Y. Abnormal functional connectivity of the hippocampus during episodic memory retrieval processing network in amnestic mild cognitive impairment. Biological Psychiatry. 2009; 65:951–958. [PubMed: 19028382]

Benson BL, Anguera JA, Seidler RD. An explicit strategy improves performance but impairs sensorimotor adaptation. Journal of Neurophysiology. 2011; 105:2843–2851. [PubMed: 21451054]

Bernard JA, Seidler RD. Relationships between regional cerebellar volume and sensorimotor and cognitive function in young and older adults. Cerebellum. In Press.

Bernard JA, Peltier SJ, Benson BL, Wiggins JL, Jaeggi SM, Buschkuehl M, Seidler RD. Dissociable functional networks of the human dentate nucleus. Cerebral Cortex. In Press.

Bernard JA, Seidler RD, Hassevoort KM, Benson BL, Welsh RC, Wiggins JL, Peltier SJ. Resting-state cortico-cerebellar functional connectivity networks: a comparison of anatomical and self-organizing map approaches. Frontiers in Neuroanatomy. 2012; 6:31. [PubMed: 22907994]

Biswal B, Yetkin FZ, Haughton VM, Hyde JS. Functional connectivity in the motor cortex of resting human brain using echo-planar MRI. Magnetic Resonance in Medicine. 1995; 34:537–541. [PubMed: 8524021]

Bo J, Borza V, Seidler RD. Age-related declines in visuospatial working memory correlate with deficits in explicit motor sequence learning. Journal of Neurophysiology. 2009; 102:2744–2754. [PubMed: 19726728]

Bostan AC, Dum RP, Strick PL. The basal ganglia communicate with the cerebellum. Proceedings of the National Academy of Sciences of the United States of America. 2010; 107:8452–8456. [PubMed: 20404184]

Buckner RL, Krienen FM, Castellanos A, Diaz JC, Yeo BT. The organization of the human cerebellum estimated by intrinsic functional connectivity. Journal of Neurophysiology. 2011; 106:2322–2245. [PubMed: 21795627]

Coxon JP, Goble DJ, Van Impe A, De Vos J, Wenderoth N, Swinnen SP. Reduced basal ganglia function when elderly switch between coordinated movement patterns. Cerebral Cortex. 2010; 20:2368–2379. [PubMed: 20080932]

Craik FI. Memory changes in normal aging. Current Directions in Psychological Science. 1994; 3:155–158.

Damoiseaux JS, Beckman CF, Sanz Arigita EJ, Barkhof F, Scheltens Ph, Stam CJ, Rombouts SARB. Reduced resting-state brain activity in the “default network” in normal aging. Cerebral Cortex. 2008; 18:1856–1864. [PubMed: 18063564]

Desmond JE, Chen SHA, Shieh PB. Cerebellar transcranial magnetic stimulation impairs verbal working memory. Annals of Neurology. 2005; 8:53–560.

D’Esposito M, Deouell LY, Gazzaley A. Alterations in the BOLD fMRI signal with ageing and disease: a challenge for neuroimaging. Nature Reviews Neuroscience. 2003; 4:863–872.

Diedrichsen J. A spatially unbiased atlas template of the human cerebellum. NeuroImage. 2006; 33:127–138. [PubMed: 16904911]

Diedrichsen J, Balsters JH, Flavell J, Cussans E, Ramnani N. A probabilistic MR atlas of the human cerebellum. NeuroImage. 2009; 46:39–46. [PubMed: 19457380]

Fearnly JM, Lees AJ. Aging and parkinsons-disease-substantia-nigra regional selectivity. Brain. 1991; 114:2283–2301. [PubMed: 1933245]

Glover GH, Li TQ, Ress D. Image-based method for retrospective correction of physiological motion effects in fMRI:RETROICOR. Magnetic Resonance in Medicine. 2000; 44:162–167. [PubMed: 10893535]

Glover GH, Law CS. Spiral-in/out BOLD fMRI for increased SNR and reduced susceptibility artifacts. Magnetic Resonance in Medicine. 2001; 46:515–522. [PubMed: 11550244]

Greicius MD, Krasnow B, Reiss AL, Menon V. Functional connectivity in the resting brain: a network analysis of the default mode hypothesis. Proceedings of the National Academy of Sciences of the United States of America. 2003; 100:253–258. [PubMed: 12506194]

Habas C, Kamdar N, Nguyen D, Prater K, Beckmann CF, Menon V, Greicius MD. Distinct cerebellar contributions to intrinsic connectivity networks. Journal of Neuroscience. 2009; 29:8586–8594. [PubMed: 19571149]

Heath RG, Harper JW. Ascending projections of the cerebellar fastigial nucleus to the hippocampus, amygdala, and other temporal lobe sites: evoked potential and histological studies in monkeys and cats. Expiremental Neurology. 1974; 45:2682–2687.

Heuninckx S, Wenderoth N, Debaere F, Peeters R, Swinnen SP. Neural basis of aging: the penetration of cognition into action control. The Journal of Neuroscience. 2005; 25:6787–6796. [PubMed: 16033888]

Heuninckx S, Wenderoth N, Swinnen SP. Systems neuroplasticity in the aging brain: recruiting additional neural resources for successful motor performance in elderly persons. The Journal of Neuroscience. 2008; 28:91–99. [PubMed: 18171926]

Hoogendam YY, van der Geest JN, van der Lijn F, van der Lugt A, Niessen WJ, Krestin GP, Ikram MA. Determinants of cerebellar and cerebral volume in the general elderly population. Neurobiology of Aging. In press.

Hoshi E, Tremblay L, Féger J, Carras P, Strick PL. The cerebellum communicates with the basal ganglia. Nature Neuroscience. 2005; 8:1491–1493.

Imamizu H, Miyauchi S, Tamada T, Sasaki Y, Takino R, Pütz B, Kawato M. Human cerebellar activity reflecting an acquired internal model of a new tool. Nature. 2000; 403:192–195. [PubMed: 10646603]

Inoue K, Kawashima R, Satoh K, Kinomura S, Sugiura M, Goto R, Fukuda H. A PET study of visuomotor learning under optical rotation. NeuroImage. 2000; 11:505–516. [PubMed: 10806036]

Jenkinson M, Banniseter P, Brady M, Smith S. Improved optimization for the robust and accurate linear registration and motion correction of brain images. NeuroImage. 2002; 17:825–841. [PubMed: 12377157]

Kelly C, de Zubicaray G, Di Martino A, Copland DA, Reiss PT, Klein DE, McMahon K. L-Dopa modulates functional connectivity in striatal cognitive and motor networks: a double-blind placebo controlled study. Journal of Neuroscience. 2009; 29:7364–7378. [PubMed: 19494158]

Kelly RM, Strick PL. Cerebellar loops with motor cortex and prefrontal cortex of a nonhuman primate. Journal of Neuroscience. 2003; 23:8432–8444. [PubMed: 12968006]

Krienen FM, Buckner RL. Segregated fronto-cerebellar circuits revealed by intrinsic functional connectivity. Cerebral Cortex. 2009; 19:2485–2497. [PubMed: 19592571]

Kwak Y, Peltier S, Bohnen NI, Müller MLTM, Dyalu P, Seidler RD. Altered resting state cortico-striatal connectivity in mild to moderate stage Parkinson's disease. Frontiers in Systems Neuroscience. 2010; 4:143. [PubMed: 21206528]

Langan J, Peltier SJ, Bo J, Fling BW, Welsh RC, Seidler RD. Functional implications of age differences in motor system connectivity. Frontiers in Systems Neuroscience. 2010; 4:1–11. [PubMed: 20204156]

Maguire EA, Frith CD. Aging affects the engagement of the hippocampus during autobiographical memory retrieval. Brain. 2003; 126:1511–1523. [PubMed: 12805116]

Mattay VS, Fera F, Tessitore A, Hariri AR, Das S, Callicott JH, Weinberger DR. Neurophysiological correlates of age-related changes in human motor function. Neurology. 2002; 58:630–635. [PubMed: 11865144]

McGeer PL, McGeer EG, Suzuki JS. Aging and extrapyramidal function. Archives of Neurology. 1977; 34:33–35. [PubMed: 12731]

Middleton FA, Strick PL. Cerebellar projections to the prefrontal cortex of the primate. The Journal of Neuroscience. 2001; 21:700–712. [PubMed: 11160449]

Naccarato M, Calautti C, Jones PS, Day DJ, Carpenter TA, Baron JC. Does healthy aging affect the hemispheric activation balance during paced index-to-thumb opposition task? An fMRI study. NeuroImage. 2006; 32:1250–1256. [PubMed: 16806984]

Nasreddine ZS, Phillips NA, Bédirian V, Charbonneau S, Whitehead V, Collin I, Cherktow H. The Montreal Cognitive Assesment, MoCA: a brief screening tool for mild cognitive impairment. Journal of the American Geriatrics Society. 2005; 53:695–699. [PubMed: 15817019]

Nichols T, Hayasaka S. Controlling the familywise error rate in functional neuroimaging: a comparative review. Statistical Methods in Medical Research. 2003; 12:419–446. [PubMed: 14599004]

Oppenheim, A.; Schafer, R.; Buck, J. Discrete-Time Signal Processing. Upper Saddle River, NJ: Prentice Hall; 1999.

O'Reilly JX, Beckmann CF, Tomassini V, Ramnani N, Johansen-Berg H. Distinct and overlapping functional zones in the cerebellum defined by resting state functional connectivity. Cerebral Cortex. 2010; 20:953–965. [PubMed: 19684249]

Park DC, Reuter-Lorenz P. The adaptive brain: aging and neurocognitive scaffolding. Annual Review of Psychology. 2009; 60:173–96.

Peltier SJ, Polk TA, Noll DC. Detecting low-frequency functional connectivity in fMRI using a self-organizing map (SOM) algorithm. Human Brain Mapping. 2003; 20:220–226. [PubMed: 14673805]

Picard N, Strick PL. Motor areas of the medial wall: a review of their location and functional activation. Cerebral Cortex. 1996; 6:342–353. [PubMed: 8670662]

Powell LE, Myers AM. The activities-specific balance confidence (ABC) scale. Journal of Gerontology Series A Biological Sciences and Medical Sciences. 1995; 50A:M28–M34.

Raz N, Dupuis JH, Briggs SD, McGavran C, Acker JD. Differential effects of age and sex on the cerebellar hemispheres and the vermis: a prospective MR study. American Journal of Neuroradiology. 1998; 19:65–71. [PubMed: 9432159]

Raz N, Gunning-Dixon F, Head D, Williamson A, Acker JD. Age and sex differences in the cerebellum and the ventral pons: a prospective MR study of healthy adults. American Journal of Neuroradiology. 2001; 22:1161–1167. [PubMed: 11415913]

Reitan, RM.; Wolfson, D. The Halstead-Reitan neuropsychological test battery. Tuscon, AZ: Neuropsychology Press; 1985.

Reuter-Lorenz PA, Jonides J, Smith EE, Hartley A, Miller A, Marshuetz C, Koeppe RA. Age differences in the frontal lateralization of verbal and spatial working memory revealed by PET. Journal of Cognitive Neuroscience. 2000; 12:174–187. [PubMed: 10769314]

Salmi J, Pallesen KJ, Neuvonen T, Brattico E, Korvenoja A, Carlson S. Cognitive and motor loops of the human cerebro-cerebellar system. Journal of Cognitive Neuroscience. 2009; 22:2663–2676. [PubMed: 19925191]

Schmiedeskamp H, Newbould RD, Pisani LJ, Skare S, Glover GH, Pruessmann KP, Bammer R. Improvements in parallel imaging accelerated functional MRI using multiecho echo-planar imaging. Magnetic Resonance in Medicine. 2010; 63:959–969. [PubMed: 20373397]

Seidler RD, Bernard JA, Burutolu TB, Fling BW, Gordon MT, Gwin JT, Lipps DB. Motor control and aging: links to brain structural, functional and biochemical changes. Neuroscience and Biobehavioral Reviews. 2010; 34:721–733. [PubMed: 19850077]

Sheline YI, Raichle ME, Snyder AZ, Morris JC, Head D, Mintun MA. Amyloid plaques disrupt resting state default mode network connectivity in cognitively normal elderly. Biological Psychiatry. 2010; 67:584–587. [PubMed: 19833321]

Sternberg S. High-speed scanning in human memory. Science. 1966; 153:652–654. [PubMed: 5939936]

Stoodley CJ, Schmahmann JD. Functional topography in the human cerebellum: a meta-analysis of neuroimaging studies. NeuroImage. 2009; 4:489–501. [PubMed: 18835452]

Stoodley CJ, Valera EM, Schmahmann JD. Functional topography of the cerebellum for motor and cognitive tasks: an fMRI study. NeuroImage. 2012; 4:489–501.

Strick PL, Dum RP, Fiex JA. Cerebellum and nonmotor function. Annual Review of Neuroscience. 2009; 32:413–434.

Teasedale N, Bard C, Fleury M, Young DE, Proteau L. Determining movement onsets from temporal series. Journal of Motor Behavior. 1993; 25:97–106. [PubMed: 15064201]

Van Dijk KRA, Sabuncu MR, Buckner RL. The influence of head motion on intrinsic functional connectivity MRI. NeuroImage. 2012; 59:431–438. [PubMed: 21810475]

Wiggins JL, Bedoyan JK, Peltier SJ, Ashinoff S, Carrasco M, Weng SJ, Welsh RC, Martin DM, Monk CS. The impact of serotonin transporter (5-HTTLPR) genotype on the development of resting-state functional connectivity in children and adolescents: a preliminary report. Neuroimage. 2012; 59:2760–2770. [PubMed: 22032950]

Wiggins JL, Peltier SJ, Ashinoff S, Weng SJ, Carrasco M, Welsh RC, Lord C, Monk CS. Using a self-organizing map algorithm to detect age-related changes in functional connectivity during rest in autism spectrum disorders. Brain Research. 2011; 22:187–197. [PubMed: 21047495]

Wing AM, Kristofferson AB. The timing of interresponse intervals. Perception and Psychophysics. 1973; 13:455–460.

Woodruff-Pak DS, Vogel RW III, Ewers M, Coffey J, Boyko OB, Lemieux SK. MRI-assessed volume of cerebellum correlates with associative learning. Neurobiology of Learning and Memory. 2001; 76:342–357. [PubMed: 11726241]

Wu T, Zang Y, Wang L, Long X, Hallett M, Chen Y, Chan P. Aging influence on functional connectivity of the motor network in the resting state. Neuroscience Letters. 2007; 42:164–168. [PubMed: 17611031]

Highlights

- We investigated age differences in resting state cortico-cerebellar networks
- Older adults showed widespread decreases in cortico-cerebellar connectivity
- Cerebellar connectivity with the basal ganglia and medial temporal lobe is impacted
- Cerebellar connectivity relates to motor and cognitive behavior in older adults

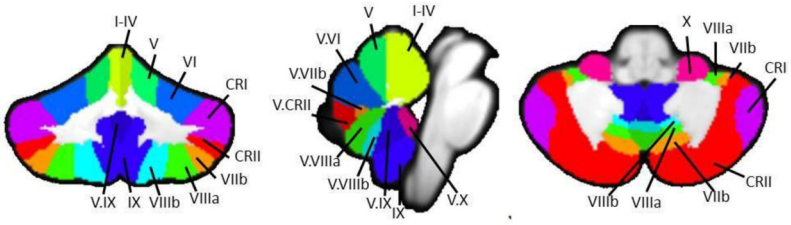

Figure 1. Masks used as seed regions for connectivity analysis

The 17 lobular regions, as defined by the SUIT atlas (Diedrichsen, 2006; Diedrichsen et al., 2009) overlaid on a coronal (left), midsaggital (center), and axial (left) slices. Labels indicate the right hemisphere and vermal seeds used in this analysis. Adapted from Bernard and Seidler (In Press), Figure 1.

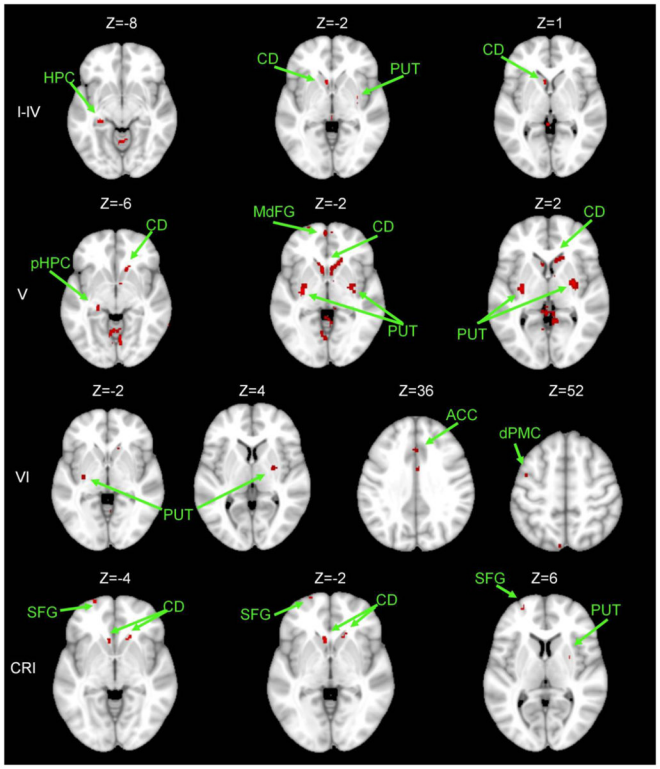

Figure 2. Areas exhibiting greater connectivity with cerebellar lobules I – Crus I in young adults versus older adults

Axial slices are presented, with the left hemisphere presented on the left. All results are thresholded using an uncorrected p<.001, and the clusters contain at least 10 voxels. CD: caudate; dPMC: dorsal pre-motor cortex; HPC: hippocampus; pHPC: parahippocampal gyrus; PUT: putamen; SFG: superior frontal gyrus.

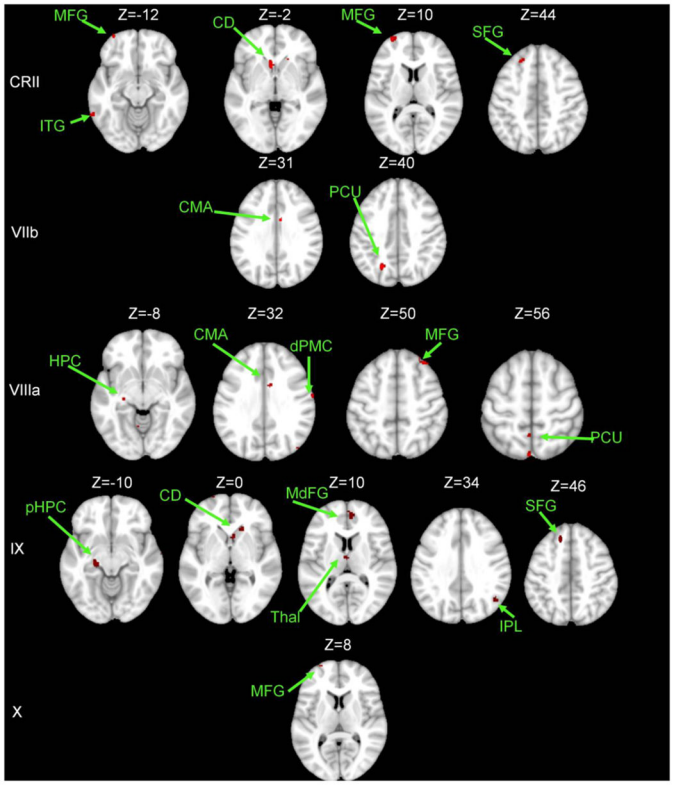

Figure 3. Areas exhibiting greater connectivity with cerebellar lobules Crus II – X in young adults versus older adults

Axial slices are presented, with the left hemisphere presented on the left. All results are thresholded using an uncorrected p<.001, and the clusters contain at least 10 voxels.. CD: caudate; CMA: cingulate motor area; dPMC: dorsal pre-motor cortex; HPC: hippocampus; IPL: inferior parietal lobule; ITG: inferior temporal gyrus; MdFG: medial frontal gyrus; MFG: middle frontal gyrus; PCU: precuneus; pHPC: parahippocampal gyrus; SFG: superior frontal gyrus; Thal: thalamus.

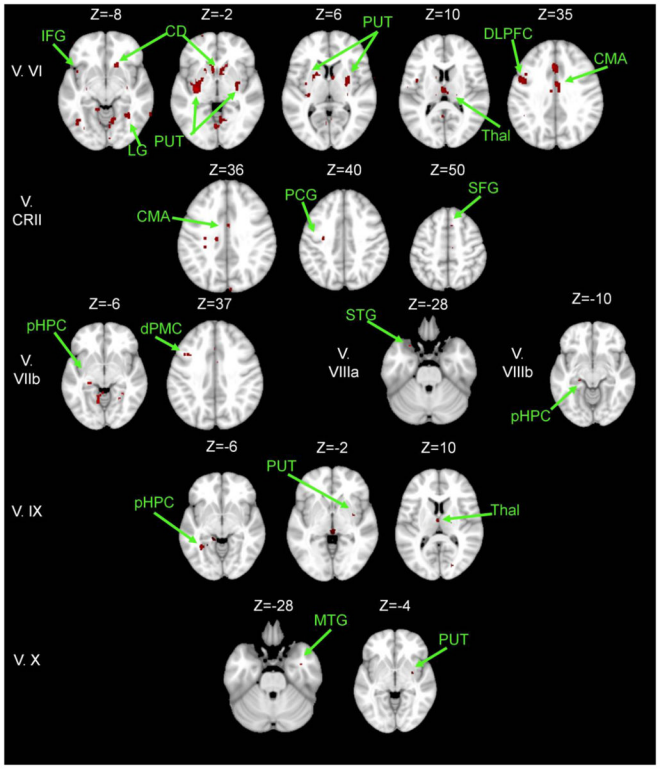

Figure 4. Areas exhibiting greater connectivity with lobules of the cerebellar vermis in young adults versus older adults

Axial slices are presented, with the left hemisphere presented on the left. All results are thresholded using an uncorrected p<.001, and the clusters contain at least 10 voxels. CD: caudate; CMA: cingulate motor area; DLPFC: dorso-lateral prefrontal cortex; dPMC: dorsal pre-motor cortex; HPC: hippocampus; MTG: middle temporal gyrus; PCG: pre-central gyrus; pHPC: parahippocampal gyrus; IFG: inferior frontal gyrus; LG: lingual gyrus; PUT: putamen; SFG: superior frontal gyrus; STG: superior temporal gyrus; Thal: Thalamus.

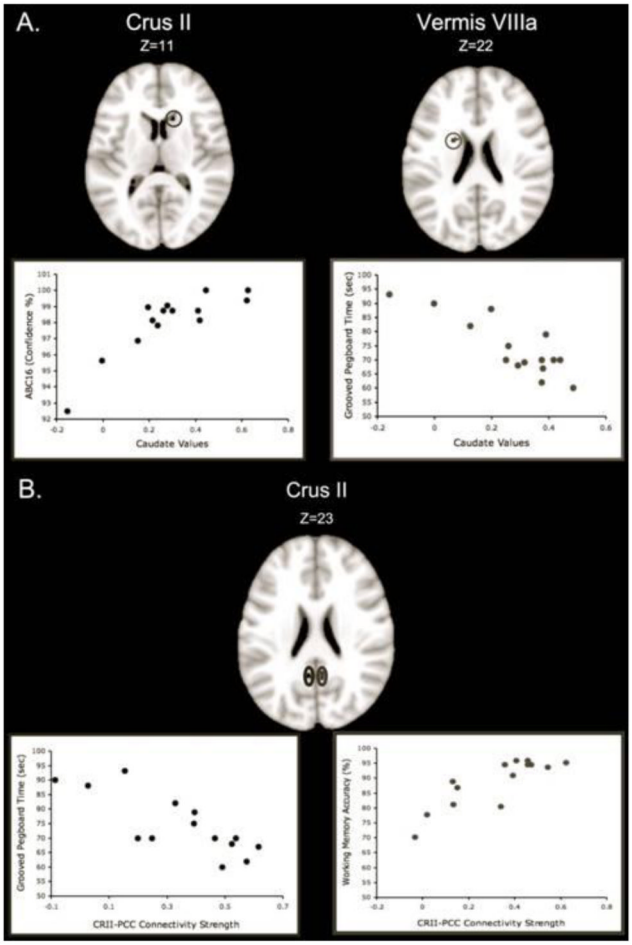

Figure 5. Functional connectivity and behavior in older adults

A. Representative correlations between sensorimotor performance and connectivity strength between the cerebellum and caudate. Connectivity between Crus II and the caudate was positively correlated with balance confidence, while connectivity between Vermis lobule VIIIa was negatively correlated with the time taken to complete the Grooved pegboard. Stronger connectivity was associated with better task performance. **B.** Crus II connectivity with the posterior cingulate predicts sensorimotor and cognitive behavioral performance. Representative example correlations between Crus II and PCC connectivity strength and time to complete the grooved pegboard (left), and working memory accuracy (right). Greater connectivity strength was associated with better task performance. CRII: Crus II; PCC: Posterior-cingulate cortex.

Table 1

MNI coordinates of the local maxima of cerebellar regions showing functional connectivity with the lobules of the right cerebellar hemisphere and vermis in older adults

Negative and positive x-values indicate locations in the left and right hemispheres, respectively. All results are family-wise error corrected, p<.005 and clusters were at least 100 voxels.

Seed	Region	MNI Coordinates			T-Value	Cluster Size
		X	Y	Z		
Lobules I–IV (n=35)	Lobules I–IV	10	−43	−15	30.95	76537
	Lobule VIIIa	28	−54	−55	9.29	411
Lobule V (n=35)	Lobule V	10	−55	−11	24.91	70208
	Crus I	34	−78	−31	9.15	473
	Crus I	−40	−76	−27	8.92	130
Lobule VI (n=35)	Lobule VI	21	−57	−20	28.7	138944
	Lobule VIIIa	−29	−60	−60	10.61	522
Crus I (n=34)	Crus I	48	−73	−30	21.19	99216
	Crus II	−48	−54	−45	8.47	185
Crus II (n=34)	Crus II	13	−87	−29	16.16	69989
	Brainstem	11	−31	5	9.79	374
		−4	−28	−2	9.23	828
		12	−27	−7	8.5	271
	Lobule X	27	−38	−41	8.51	318
Lobule VIIb (n=21)	Lobule VIIb	35	−67	−54	21.34	2740
	Crus II	−21	−80	−51	13.55	631
		9	−79	−35	11.65	113
	Lobules I–IV	5	−55	−16	13.53	505
	Vermis VIIIa	0	−70	−37	13.3	224
	Vermis VI	−2	−70	−23	12.17	172
	Lobule VI	30	−70	−20	11.48	105
		25	−61	−15	10.84	398
	Vermis IX	−2	−57	−36	10.84	141

Seed	Region	MNI Coordinates			T-Value	Cluster Size
		X	Y	Z		
	Lobule VIIIa	34	−49	−56	10.41	250
	Lobule VIIIb	18	−49	−52	10.37	113
Lobule VIIIa (n=22)	Lobule VIIIa	29	−62	−58	19.09	4712
	Lobule VI	−26	−68	−22	14.92	516
		20	−73	−15	14.18	778
		7	−69	−12	12.14	181
	Lobules I–IV	−3	−54	−15	12.69	306
	Crus II	−14	−79	−49	11.18	242
Lobule VIIIb (n=22)	Lobule VIIIb	19	−47	−51	12.97	1959
Lobule IX (n=31)	Lobule IX	5	−53	−45	36.43	38689
	Crus II	32	−71	−44	10.34	482
	Lobule V	−17	−51	−24	8.5	220
Lobule X (n=35)	Lobule X	21	−38	−47	64.77	2162
		−23	−36	−44	10.47	179
	Lobule VI	7	−70	−16	10.23	282
	Vermis IX	−2	−52	−37	8.94	274
	Crus II	−16	−76	−35	8.92	486
	Crus I	13	−76	−29	8.02	138
Vermis VI (n=35)	Vermis VI	0	−69	−21	39.7	79753
	Lobules I–IV	27	−35	−36	9.3	187
	Lobule VIIIa	−32	−59	−61	8.7	369
	Crus I	−50	−71	−30	7.91	183
Vermis Crus II (n=35)	Vermis Crus II	1	−74	−31	189.64	4697
	Lobule VI	−21	−65	−32	9.27	269
		29	−70	−14	8.9	199
	Crus II	−17	−83	−46	9.21	146
	Crus I	−19	−80	−31	9.21	399
	Lobule V	−6	−63	−14	9	210

Seed	Region	MNI Coordinates			T-Value	Cluster Size
		X	Y	Z		
		−14	−54	−23	8.32	167
	Lobule IX	−2	−57	−42	8.18	132
Vermis VIIb (n=34)	Vermis VIIb	−3	−67	−31	26.59	1313
	Lobules I–IV	3	−53	−21	10.65	394
Vermis VIIIa (n=35)	Vermis VIIIa	0	−65	−35	61.68	73968
	Brainstem	7	−28	5	10.57	1539
		−6	−33	6	9.53	532
Vermis VIIIb (n=35)	Vermis VIIIb	2	−63	−41	57.51	12746
	Lobules I–IV	−5	−56	−15	12.78	21785
	Crus I	46	−72	−28	9.86	497
	Lobule VIIIa	−30	−36	−46	9.17	404
	Brainstem	−3	−41	−1	9.16	890
		12	−28	−12	8.11	162
	Lobule X	19	−41	−46	9.04	154
	Lobule VIIIb	23	−45	−51	8.93	119
	Lobule VI	−35	−42	−37	8.93	272
Vermis IX (n=35)	Vermis IX	−2	−54	−36	109.3	60786
	Lobule X	26	−38	−43	9.36	262
	Brainstem	2	−40	−1	9.33	873
Vermis X (n=35)	Vermis X	0	−48	−35	415.3	3914
	Lobule V	−24	−31	−34	9.67	299
	Vermis VI	4	−74	−18	8.57	161

Table 2

MNI coordinates of the local maxima of brain regions showing functional connectivity with the lobules of the right cerebellar hemisphere and vermis in the older adults

Negative and positive x-values indicate locations in the left and right hemispheres, respectively.

Seed	Region	BA	MNI Coordinates			T-Value	Cluster Size
			X	Y	Z		
Lobules I–IV * (n=35)**	Parahippocampal Gyrus	34	20	0	−12	13.92	1193
	Superior Temporal Gyrus	41	−52	−20	6	12.9	477
		38	−52	16	−8	11.1	217
	Middle Frontal Gyrus	9	−36	50	28	12.35	327
			40	46	26	9.96	140
	Subcallosal Gyrus	34	−14	6	−14	11.36	440
	Hippocampus	-	34	−16	−18	11.2	506
	Middle Frontal Gyrus (dPMC)	6	38	0	60	11.03	129
	Caudate	-	−12	8	6	10.44	122
	Anterior Cingulate Cortex	32	−8	42	14	10.26	434
	Inferior Parietal Lobule	40	50	−30	24	9.15	105
Lobule V * (n=35)**	Middle Frontal Gyrus	9	−36	50	28	12.97	335
	Superior Temporal Gyrus	22	48	6	2	11.06	646
		41	−44	−30	4	10.26	256
		38	−50	16	−6	9.52	105
	Anterior Cingulate Cortex	25	0	18	−2	10.58	118
	Parahippocampal Gyrus	34	−14	4	−14	10.29	109
	Precentral Gyrus	4	40	−16	42	10.05	115
			−36	−18	40	9.21	109
	Subcallosal Gyrus	34	20	6	−12	9.47	106
	Medial Frontal Gyrus	10	−10	42	10	9.15	189
Lobule VI * (n=35)**	Middle Frontal Gyrus	9	−38	48	28	15.16	1484
	Superior Temporal Gyrus	22	−56	12	−2	14.39	409
	Middle Frontal Gyrus (dPMC)	6	40	0	56	11.72	247

Seed	Region	BA	MNI Coordinates			T-Value	Cluster Size
			X	Y	Z		
	Superior Frontal Gyrus	10	38	52	22	11.11	360
	Post-Central Gyrus	3	54	−24	42	10.93	381
	Anterior Cingulate Cortex	32	−10	40	10	10.89	342
		24	0	20	2	10.87	228
	Inferior Parietal Lobule	40	−60	−34	22	10.53	304
	Amygdala	-	−28	−10	−10	10.22	216
	Pre & Post-Central Gyrus	2 & 4	−52	−28	38	9.84	216
Crus I * (n=34)**	Superior Frontal Gyrus	9	−30	56	29	11.58	265
		8	−26	22	50	10.59	217
	Precuneus	7	0	−74	32	11.32	1469
	Caudate Head	--	12	26	−4	10.11	114
Crus II * (n=34)**	Precuneus	7	0	−58	48	10.94	1197
	Thalamus, Ventral Anterior Nucleus	--	−12	−4	12	10.85	335
	Caudate	--	14	12	14	10.61	248
	Thalamus, Pulvinar	--	20	−24	18	10.43	417
	Supramarginal Gyrus	40	−54	−58	30	10.36	237
	Angular Gyrus	39	42	−60	38	10.14	416
	Anterior Cingulate Cortex	32	−8	36	22	9.95	212
	Medial Frontal Gyrus	10	4	54	4	9.58	165
		11	4	44	−14	9.3	131
Lobule VIIIa * (n=22)	Anterior Cingulate Cortex	32	−14	24	26	12.24	104
Lobule VIIIb * (n=22)	Precuneus	7	−2	−78	38	12.01	228
Lobule IX * (n=31)**	Thalamus, Ventral Lateral Nucleus	--	14	−10	14	13.44	329
	Anterior Cingulate Cortex	32	−8	40	12	11.32	212
	Caudate	--	−12	10	12	10.81	304
	Superior Temporal Gyrus	39	44	56	−18	9.75	148
Vermis VI * (n=35)**	Thalamus	--	−10	−2	10	12.98	865
	Middle Frontal Gyrus	10	−30	56	20	11.35	479

Seed	Region	BA	MNI Coordinates			T-Value	Cluster Size
			X	Y	Z		
	Cingulate Motor Area	32	−6	14	34	10.26	755
	Inferior Parietal Lobule	40	54	−28	22	10.1	175
	Claustrum	--	28	24	2	9.9	123
	Superior Frontal Gyrus	9	38	46	30	9.31	271
	Precentral Gyrus	6	58	0	8	8.91	136
Vermis VIIIa* (n=35)**	Thalamus, Ventral Lateral Nucleus	--	−8	−8	8	14.93	1418
	Posterior Cingulate Cortex	31	4	−38	40	12.18	2032
	Cingulate Motor Area	24	4	−20	42	11.26	390
	Superior Occipital Gyrus	19	36	−72	22	10.35	147
	Anterior Cingulate Cortex	32	−8	32	24	10.22	191
	Middle Frontal Gyrus	10	−28	42	20	10.03	613
			32	46	18	9.75	378
	Supramarginal Gyrus	40	52	−46	36	9.54	256
Vermis VIIIb* (n=35)**	Precuneus	19	−4	80	40	11.87	269
	Cuneus	17	4	−82	6	10.9	129
	Thalamus, Medial Dorsal Nucleus	--	12	−18	6	10.5	174
	Caudate	--	−22	2	22	9.54	174
Vermis IX* (n=35)**	Thalamus, Ventral Anterior Nucleus	--	14	−8	13	14.92	2079
	Precuneus	7	0	−74	46	14.85	3039
	Supramarginal Gyrus	40	56	−50	34	10.36	354

All results are family-wise error corrected,

* p<.05,

** p<.01,

*** p<.005, and clusters were at least 100 voxels.

Table 3

MNI coordinates of the local maxima of cerebellar regions showing greater functional connectivity in young adults when lobules of the right cerebellar hemisphere were used as seeds

Negative x-values indicate locations in the left hemisphere, while positive x-values indicate locations in the right hemisphere. All results are uncorrected p<.001, with a minimum cluster size of 10 voxels.

Seed	Region	MNI Coordinates			T-Value	Cluster Size
		X	Y	Z		
Lobules I-IV (YA n=33 OA n=35)	Lobules I–IV	18	−35	−22	5.59	6167
		−17	−40	−17	4.21	122
		−10	−44	−8	3.4	19
	Lobule V	−14	−47	−41	4.13	99
	Crus I	−43	−43	−28	4.09	256
	Lobule X	−17	−36	−48	3.93	92
	Brainstem	−1	−33	−1	3.86	141
		11	−31	−40	3.68	146
		−12	−28	−40	3.44	35
	Vermis VIIIa	8	−66	−3	3.8	65
	Dentate Nucleus	−19	−58	−38	3.7	15
		−24	−52	−40	3.29	11
	Lobule IX	13	−50	−41	3.6	69
	Lobule VI	16	−60	−16	3.53	23
		−11	−66	−21	3.52	36
		−18	−55	−15	3.41	18
		−22	−62	−18	3.39	17
Lobule V (YA n=33 OA n=35)	Lobule V	15	−51	−14	5.6	16132
	Lobule VI	37	−62	−20	4.54	681
		29	−55	−26	3.63	21
		22	−58	−27	3.56	32
	Brainstem	12	−32	−39	4.45	415
		3	−28	3	4.45	211

Seed	Region	MNI Coordinates			T-Value	Cluster Size
		X	Y	Z		
		10	−32	1	4.2	163
		−3	−33	−15	4	129
		−1	−38	−39	3.43	18
	Lobule X	−17	−41	−46	4.38	234
		23	−38	−42	3.64	77
	Crus I	49	−62	−30	4.1	287
		−42	−54	−27	3.76	49
		−45	−68	−28	3.58	15
		29	−85	−26	3.51	15
	Lobule VIIb	−14	−70	−41	3.74	64
	Dentate Nucleus	−25	−53	−42	3.6	43
	Vermis VIIIa	4	−63	−32	3.57	123
	Lobule VIIIb	−27	−41	−56	3.54	12
Lobule VI (YA n=33 OA n=35)	Lobule VI	24	−60	−20	5.79	6044
		−12	−67	−17	5.37	1461
		−31	−71	−20	3.96	157
	Brainstem	0	−34	−30	4.57	849
		13	−32	−37	4.45	239
		−17	−31	−32	3.81	79
		−10	−23	−42	3.57	15
		6	−36	−29	3.51	15
	Crus I	−48	−45	−25	4.48	644
		32	−60	−34	3.92	81
		−45	−68	−28	3.8	119
		9	−73	−31	3.47	18
	Lobule IX	−12	−47	−41	3.87	72
	Lobules I–IV	4	−57	−3	3.71	238
	Lobule VIIIb	−26	−41	−56	3.47	11

Seed	Region	MNI Coordinates			T-Value	Cluster Size
		X	Y	Z		
	Lobule X	23	−38	−41	3.41	16
	Lobule V	14	−55	−12	3.32	14
Crus I (YA n=30 OA n=34)	Crus I	24	−84	−24	5.76	2935
		−45	−67	−28	4.06	101
		42	−70	−35	3.63	79
		−43	−56	−28	3.47	25
	Brainstem	−17	−31	−31	4.3	128
		0	−35	−30	4.27	235
		11	−39	−44	3.43	13
	Lobule IX	8	−53	−39	4.25	332
	Lobule V	−22	−45	−19	3.56	26
	Lobules I–IV	28	−32	−27	3.36	15
Crus II (YA n=25 OA n=34)	Crus I	46	−71	−40	5.4	5522
		−20	−91	−29	4.6	483
		−27	−81	−26	4.41	103
		−32	−84	−34	4.08	229
		41	−66	−26	3.71	30
		−7	−84	−24	3.62	49
	Crus II	−9	−84	−42	4.83	186
		−22	−76	−38	3.92	94
		−27	−77	−49	3.52	19
		−41	−46	−42	3.49	10
	Lobule X	−15	−42	−44	4.8	445
	Lobule IX	7	−54	−38	4.79	451
	Lobule V	−22	−48	−18	3.87	66
		−27	−38	−22	3.74	76
		23	−37	−23	3.43	11
	Brainstem	0	−35	−31	3.74	49

Seed	Region	MNI Coordinates			T-Value	Cluster Size
		X	Y	Z		
		−11	−25	−37	3.38	14
Lobule VIIb (YA n=20 OA n=21)	Lobule VIIb	12	−77	−48	4.62	173
		31	−74	−54	4.09	81
		43	−54	−53	3.77	24
	Crus I	49	−63	−27	3.98	118
		28	−87	−26	3.97	106
		−44	−54	−26	3.79	60
	Lobule VI	−28	−58	−24	3.85	50
	Lobule IX	12	−59	−49	3.73	71
	Lobule VIIIa	−30	−47	−54	3.68	24
Lobule VIIIa (YA n=19 OA n=22)	Lobule VIIIa	−28	−54	−58	5.39	896
		32	−56	−56	4.72	238
		20	−69	−61	3.83	28
	Lobule VI	−26	−51	−23	4.75	841
		−5	−74	−12	4.68	1429
		30	−57	−33	3.71	70
		23	−57	−18	3.6	14
		30	−40	−40	3.53	14
	Brainstem	−4	−29	4	4.37	73
		7	−35	1	3.72	47
		−17	−27	−11	3.46	12
	Lobules I–IV	3	−55	−1	4.23	254
		−1	−45	−7	3.48	14
	Crus II	12	−79	−46	4.17	72
		50	−62	−46	3.85	14
	Crus I	−44	−55	−25	3.82	13
		27	−87	−26	3.65	41
	Lobule VIIIb	14	−60	−51	3.7	63

Seed	Region	MNI Coordinates			T-Value	Cluster Size
		X	Y	Z		
	Dentate Nucleus (Middle)	20	−60	−36	3.52	10
Lobule VIIIb (YA n=19 OA n=22)	Lobule VIIIb	22	−45	−49	5.35	1256
		−24	−44	−46	4.2	223
		−14	−52	−62	3.73	14
	Lobule VIIIa	−28	−53	−58	4.22	82
		−35	−46	−59	3.77	19
		35	−56	−57	3.71	16
		−34	−51	−52	3.47	18
	Crus I	28	−85	−26	4.19	282
	Crus II	49	−64	−46	4.08	91
	Lobule V	−24	−49	−19	3.82	142
	Lobule VIIb	43	−4	−53	3.81	23
	Lobule I–IV	5	−52	1	3.68	36
	Lobule X	−17	−40	−45	3.8	18
	Brainstem	1	−24	−10	3.46	11
Lobule IX (YA n=23 OA n=31)	Lobule IX	5	−54	−52	7.97	2407
	Crus I	−31	−81	−26	4.95	939
		21	−88	−24	4.56	393
		47	−60	−26	4.04	93
		35	−71	−38	4.03	107
	Brainstem	−16	−23	−15	4.77	237
	Brainstem	0	−36	−31	3.71	38
	Crus II	15	−85	−40	4.1	93
	Lobule X	−17	−37	−44	3.65	33
	Crus I	40	−60	−41	3.45	11
Lobule X (YA n=33 OA n=35)	Lobule X	22	−37	−45	8.48	1161
		−14	−41	−45	5.36	2694
	Crus I	42	−80	−40	4.47	248

Seed	Region	MNI Coordinates			T-Value	Cluster Size
		X	Y	Z		
		46	−62	−44	3.77	17
		21	−88	−24	3.67	41
		−28	−82	−26	3.59	70
		−23	−49	−19	4.26	53
		−5	−62	−19	4.05	528
	Lobule V	−12	−47	−12	3.68	44
		31	−39	−27	3.6	29
		−21	−42	−16	3.48	32
		−30	−60	−22	4.16	97
	Lobule VI	−30	−71	−24	3.94	155
		28	−66	−18	3.69	14
		−16	−28	−32	3.99	96
		13	−29	−44	3.89	42
	Brainstem	−1	−33	−54	3.65	123
		8	−31	−11	3.42	11
	Dorsal Dentate Nucleus	−12	−51	−35	3.85	123
	Ventral Dentate Nucleus	−26	−53	−43	3.83	45
	Lobules I–IV	5	−51	0	3.62	19

Table 4

MNI coordinates of the local maxima of cerebellar regions showing greater functional connectivity in young adults when lobules of the cerebellar vermis were used as seeds

Negative x-values indicate locations in the left hemisphere, while positive x-values indicate locations in the right hemisphere. All results are uncorrected p<.001, with a minimum cluster size of 10 voxels.

Seed	Region	MNI Coordinates			T-Value	Cluster Size
		X	Y	Z		
Vermis VI (YA n=33 OA n=35)	Vermis VI	2	−70	−17	7.12	3104
	Brainstem	15	−32	−37	4.46	414
		5	−33	−19	3.82	32
		0	−36	−32	3.68	94
	Lobule V	−15	−45	−12	4.01	83
		−20	−51	−16	3.84	95
		8	−61	−6	3.4	16
	Lobule VI	33	−64	−22	3.66	47
	Crus II	49	−70	−48	3.62	37
	Crus I	−7	−73	−32	3.49	31
		51	−66	−45	3.38	10
	Lobule IX	−13	−47	−42	3.31	10
Vermis Crus II (YA n=33 OA n=35)	Vermis Crus II	1	−75	−31	17.2	1239
	Lobule VI	−20	−58	−14	4.56	243
		−12	−68	−14	3.91	150
		−32	−58	−21	3.89	70
		31	−42	−35	3.73	46
		−38	−38	−36	3.59	13
		19	−60	−27	3.41	10
	Brainstem	4	−37	−47	4.09	216
		−15	−39	−41	3.75	30
	Vermis VI	6	−75	−20	4.03	43
	Crus II	−10	−75	−42	3.63	57

Seed	Region	MNI Coordinates			T-Value	Cluster Size
		X	Y	Z		
	Crus I	−41	−46	−41	3.52	20
		45	−62	−27	3.44	13
	Louble VIIIb	17	−57	−49	3.51	51
	Lobule IX	−11	−46	−42	3.36	19
Vermis VIIb (YA n=33 OA n=34)	Vermis VIIb	−1	−68	−31	18.37	739
	Lobule VI	38	−60	−21	4.94	209
		29	−49	−26	3.82	85
		−25	−54	−17	3.61	79
		28	−54	−20	3.47	14
	Lobules I–IV	19	−37	−20	4.88	213
		12	−49	−13	3.56	24
	Crus I	48	−65	−26	4.22	121
		−41	−48	−30	3.86	45
		53	−59	−32	3.67	30
		34	−73	−23	3.66	15
		−53	−59	−32	3.65	40
		39	−60	−40	3.49	11
	Lobule VIIIa	17	−65	−43	4.04	160
	Lobule VIIIb	16	−54	−51	3.76	67
	Brainstem	6	−25	−2	3.72	25
		2	−34	−24	3.36	13
	Lobule V	4	−62	−8	3.67	27
	Lobule IX	−7	−60	−45	3.51	15
Vermis VIIIa (YA n=33 OA n=35)	Vermis VIIIa	0	−69	−41	7.36	1382
	Lobule V	4	−63	−2	4.49	729
	Ventral Dentate	21	−61	−39	4.05	73
	Lobule VIIIb	−25	−42	−57	3.65	27
	Crus I	54	−57	−29	3.4	14

Seed	Region	MNI Coordinates			T-Value	Cluster Size
		X	Y	Z		
Vermis VIIIb (YA n=33 OA n=35)	Vermis VIIIb	0	−64	−42	11.82	982
	Lobule IX	13	−54	−36	4.12	305
	Crus I	−32	−85	−26	3.76	54
		−43	−55	−27	3.59	14
	Lobules I–IV	1	−46	−9	3.52	37
	Interposed Nuclei	−8	−56	−29	3.42	11
	Lobule IX	−9	−54	−34	3.41	11
Vermis IX (YA n=33 OA n=35)	Vermis IX	0	−55	−35	13.19	2540
	Brainstem	−3	−32	−15	5.59	2001
		1	−28	−2	4.13	168
	Crus I	−14	−90	−25	4.7	465
		48	−61	−23	4.4	273
		22	−86	−23	4.19	137
		−55	−53	−38	4.11	156
		39	−60	−40	3.69	44
		40	−76	−23	3.61	45
		−45	−58	−28	3.57	30
		54	−55	−29	3.39	17
		−29	−84	−25	3.36	12
	Lobules I–IV	−12	−40	−10	4.28	244
	Lobule X	−16	−36	−46	4.09	90
	Lobule VIIb	−14	−72	−42	4.07	54
	Lobule V	−20	−47	−19	3.66	63
		3	−60	0	3.56	20
	Lobule VI	−28	−46	−23	3.46	23
Vermis X (YA n=33 OA n=35)	Vermis X	1	−48	−35	15.42	226
	Brainstem	11	−24	−13	4	45
		2	−32	−21	3.56	36

Seed	Region	MNI Coordinates			T-Value	Cluster Size
		X	Y	Z		
Ventral		−16	−26	−11	3.55	26
		−4	−39	−27	3.53	11
		1	−33	−32	3.39	13
	Ventral	16	−64	−37	3.93	40
	Dentate	−18	−52	−39	3.55	51
	Nucleus	13	−51	−38	3.37	10
	Crus I	28	−87	−25	3.81	48
	Crus II	−16	−72	−42	3.5	16

Table 5

MNI coordinates of the local maxima of brain regions showing greater functional connectivity in young adults versus older adults when lobules of the right cerebellar hemisphere were used as seeds

Negative x-values indicate locations in the left hemisphere, while positive x-values indicate locations in the right hemisphere. All results are uncorrected p<.001, with a minimum cluster size of 10 voxels.

Seed	Region	BA	MNI Coordinates			T-Value	Cluster Size
			X	Y	Z		
Lobules I–IV (YA n=33 OA n=35)	Hippocampus	--	−2	−40	2	4.67	44
			−28	−30	−8	4.28	21
	Parahippocampal Gyrus	35	−18	−28	−12	4.48	23
	Midbrain	--	−6	−14	−2	4.07	27
	Middle Temporal Gyrus	21	56	0	−26	3.85	16
	Caudate	--	4	12	2	3.64	19
			14	22	0	3.63	10
	Putamen	--	32	−6	−2	3.58	15
Lobule V (YA n=33 OA n=35)	Putamen	--	−30	−12	0	5.73	188
			30	−6	4	5.35	340
	Thalamus	--	−6	−14	−2	4.97	89
	Caudate	--	14	22	0	4.9	300
			20	−14	22	3.96	89
			−10	−6	18	3.91	24
	Parahippocampal Gyrus	27	−22	−30	−6	4.7	113
		28	24	−28	−6	3.65	12
	Lingual Gyrus	18	42	−92	−12	4.25	17
			−2	−94	−12	4.19	16
	Medial Frontal Gyrus	10	6	62	18	4.15	34
			−2	−60	10	4.07	117
	Superior Frontal Gyrus	10	−24	−66	−4	4.14	36
	Anterior Cingulate Cortex	32	−2	34	24	4.06	169
		24	6	6	28	3.76	34

Seed	Region	BA	MNI Coordinates			T-Value	Cluster Size
			X	Y	Z		
	Middle Temporal Gyrus	39	42	−74	10	4.03	32
		21	40	−4	−26	4	25
	Superior Temporal Gyrus	39	60	−64	22	3.87	16
	Fusiform Gyrus	37	−26	−50	−6	3.44	10
Lobule VI (YA n=33 OA n=35)	Inferior Frontal Gyrus	47	54	44	−10	5.01	79
	Post-Central Gyrus	7	−6	−50	76	4.52	49
	Superior Frontal Gyrus	8	38	32	48	4.39	28
		10	−36	68	−6	4.24	31
		10	44	58	14	3.5	14
	Putamen	--	26	−6	4	4.07	42
			−32	−14	−2	3.95	46
	Dorsal Premotor Cortex	6	−42	0	52	4.05	12
	Anterior Cingulate Cortex	32	0	24	34	3.93	55
	Lingual Gyrus	18	−2	−94	−12	3.9	12
	Parahippocampal Gyrus	35	−22	−20	−19	3.62	16
Crus I (YA n=30 OA n=34)	Caudate	--	−6	20	−2	4.22	34
	Superior Frontal Gyrus	10	−24	66	−4	4.21	39
		11	2	58	−24	4.15	34
		10	−24	58	8	3.77	26
	Putamen	--	28	2	6	3.57	11
Crus II (YA n=25 OA n=34)	Middle Frontal Gyrus	10	−30	62	8	5.12	240
	Inferior Temporal Gyrus	20	−64	−50	−12	5	79
		37	64	−50	−6	4.1	29
	Caudate	--	−6	16	−2	4.7	98
			6	12	2	3.6	11
	Superior Frontal Gyrus	8	−20	34	44	4.4	35
			20	26	52	3.95	19
	Superior Temporal Gyrus	38	−26	14	−26	4.1	14

Seed	Region	BA	MNI Coordinates			T-Value	Cluster Size
			X	Y	Z		
	Parahippocampal Gyrus	28	−22	−26	−6	3.98	13
	Globus Pallidus	--	20	−2	2	3.73	22
Lobule VIIb (YA n=20 OA n=21)	Precuneus	7	−22	−62	40	4.53	59
	Cingulate Motor Area	24	6	4	30	4.48	45
	Insula	13	−54	−24	22	4.2	25
	Inferior Frontal Gyrus	46	56	38	10	4.09	14
	Middle Frontal Gyrus	8	38	34	46	4	17
Lobule VIIIa (YA n=19 OA n=22)	Middle Frontal Gyrus	8	34	34	50	5.15	62
	Dorsal Pre-Motor Cortex	6	66	−8	32	5.01	10
	Cingulate Motor Area	24	8	6	32	4.22	14
	Hippocampus	--	−26	−22	−8	3.97	22
	Precuneus	7	8	−58	60	3.8	13
			−2	−54	56	3.75	17
	Anterior Cingulate (non-motor)	24	18	−18	38	3.71	12
	Lingual Gyrus	18	8	−74	−2	3.54	10
Lobule IX (YA n=23 OA n=31)	Parahippocampal Gyrus	35	−22	−22	−10	4.36	56
	Caudate	--	16	24	0	4.35	20
			4	12	0	4.13	23
	Superior Frontal Gyrus	10	−34	62	−4	4.2	13
			−22	66	−4	4.16	25
		8 (FEF)	−14	32	46	4.04	20
	Medial Frontal Gyrus	10	6	48	12	4.19	72
	Precuneus	7	2	−60	40	3.99	28
	Middle Temporal Gyrus	39	−56	−70	26	3.97	15
	Posterior Cingulate	23	0	−54	16	3.97	26
	Post-Central Gyrus	40	−66	−22	−14	3.89	20
	Angular Gyrus	39	−46	−68	−28	3.89	19
	Inferior Parietal Lobule	39	48	−62	34	3.78	11

Seed	Region	BA	MNI Coordinates			T-Value	Cluster Size
			X	Y	Z		
Lobule X (YA n=33 OA n=35)	Thalamus (Medial Dorsal Nucleus)	--	−2	−10	10	3.77	21
	Lingual Gyrus	18	−2	−94	−12	4.51	14
	Middle Frontal Gyrus	10	−26	64	8	4.3	19
	Putamen	--	26	−6	−4	3.93	11

Table 6

MNI coordinates of the local maxima of brain regions showing greater functional connectivity in young adults versus older adults when lobules of the cerebellar vermis were used as seeds

Negative x-values indicate locations in the left hemisphere, while positive x-values indicate locations in the right hemisphere. All results are uncorrected p<.001, with a minimum cluster size of 10 voxels.

Seed	Region	BA	MNI Coordinates			T-Value	Cluster Size
			X	Y	Z		
Vermis VI (YA n=33 OA n=35)	Putamen	--	−32	−14	−2	6.09	969
			32	−12	−6	4.62	244
	Cingulate Motor Area	32	−4	22	30	5.59	968
	Dorsal Pre-Motor Cortex	6	−46	4	34	5.12	147
			−42	0	50	4.76	184
			44	2	40	4.07	25
			32	−4	56	3.90	35
			28	10	56	3.54	14
	Thalamus (Medial Dorsal Nucleus)	--	−2	−10	10	4.60	113
	Caudate	--	−6	14	02	4.56	17
	Paracentral Lobule	31	−4	−20	44	4.49	130
	Inferior Temporal Gyrus	37	66	−50	−6	4.49	46
	Supramarginal Gyrus	20	−44	−46	30	4.30	51
	Parahippocampal Gyrus	36	−18	−34	−10	4.22	36
	Superior Frontal Gyrus	10	46	58	16	4.21	24
			32	58	24	3.50	14
	Posterior Cingulate Cortex	23	−2	−56	14	4.09	59
	Inferior Frontal Gyrus	47	−42	12	−8	4.00	22
		46	56	40	10	3.98	10
	Lingual Gyrus	18	6	−88	−8	3.98	38
	Pre-Central Gyrus	43	−56	−10	10	3.97	19
	Inferior Parietal Lobule	40	−48	−38	44	3.84	47
	Uncus	28	30	−6	−22	3.79	34

Seed	Region	BA	MNI Coordinates			T-Value	Cluster Size
			X	Y	Z		
	Middle Frontal Gyrus	10	34	40	20	3.75	23
			−44	42	10	3.62	13
	DLPFC (MFG)	9	−40	12	36	3.74	10
		46	54	36	26	3.70	16
	Superior Temporal Gyrus	38	50	12	−12	3.73	28
	Middle Temporal Gyrus	39	46	−72	16	3.71	10
	Superior Occipital Gyrus	19	−36	−76	28	3.69	11
	Precuneus	7	10	−58	60	3.64	10
			12	−50	48	3.60	21
	Ventral Pre-Motor Cortex	6	−54	−2	24	3.61	18
	Post-Central Gyrus	2	−32	−36	68	3.51	10
Vermis Crus II (YA n=33 OA n=35)	Cingulate Motor Area	24	4	−2	36	4.55	175
	Posterior Cingulate Cortex	30	20	−60	12	4.27	35
	Pre-Central Gyrus	4	−32	−14	40	4.11	114
	Fusiform Gyrus	19	38	−64	−4	4.20	22
	Cuneus	18	8	−84	22	4.06	35
			−16	−86	24	3.69	11
	Middle Occipital Gyrus	19	28	−94	14	3.94	11
	Insula	13	−40	−20	20	3.93	32
	Superior Frontal Gyrus	8	8	20	50	3.77	23
Vermis VIIb (YA n=33 OA n=34)	Fusiform Gyrus	37	32	−48	−8	4.55	43
	Parahippocampal Gyrus	27	−24	−28	−8	4.54	90
		35	18	−30	−6	3.52	12
	Posterior Cingulate Cortex	30	18	−58	4	4.26	47
		31	−12	−36	40	3.74	11
	Cuneus	17	18	−82	8	4.18	16
	Anterior Cingulate Cortex	32	0	24	34	4.13	13
	Uncus	38	−24	12	−28	4.12	23

Seed	Region	BA	MNI Coordinates			T-Value	Cluster Size
			X	Y	Z		
	Middle Temporal Gyrus	37	−62	−64	4	4.06	19
	Cingulate Motor Area	24	4	0	38	3.64	17
	Dorsal Pre-Motor Cortex	9	−36	12	36	3.63	11
Vermis VIIIa (YA n=33 OA n=35)	Superior Temporal Gyrus	38	−26	16	−28	4.30	11
Vermis VIIIb (YA n=33 OA n=35)	Parahippocampal Gyrus	28	−22	−28	−10	3.93	13
Vermis IX (YA n=33 OA n=35)	Parahippocampal Gyrus	19	34	−50	−6	5.41	52
	Thalamus	--	−2	−10	10	4.51	54
			26	−24	8	4.00	23
	Cuneus	17	20	−82	10	4.29	22
	Thalamus (Ventral Lateral Nucleus)	--	20	−14	10	3.75	12
	Hippocampus	--	−26	−36	4	3.74	37
Vermis X (YA n=33 OA n=35)	Putamen	--	30	−4	4	4.22	18
	Middle Temporal Gyrus	21	38	−2	−28	3.93	13

Table 7

MNI coordinates of the local maxima of cerebellar regions showing greater functional connectivity in older adults than young adults when lobules of the cerebellar right hemisphere and vermis were used as seeds

Negative x-values indicate locations in the left hemisphere, while positive x-values indicate locations in the right hemisphere. All results are uncorrected p<.001, with a minimum cluster size of 10 voxels.

Seed	Region	MNI Coordinates			T-Value	Cluster Size
		X	Y	Z		
Lobules I–IV (YA n=33 OA n=35)	Lobule VIIIa	23	−57	−64	5.16	354
	Lobule VIIIb	−33	−69	−59	3.96	248
Lobule V (YA n=33 OA n=35)	Lobule VIIIa	22	−59	−64	5.51	365
	Lobule IX	5	−50	−63	4.31	81
Lobule VI (YA n=33 OA n=35)	Lobule VIIIa	22	−59	−64	4.29	14
Crus I (YA n=30 OA n=34)	Lobule VIIIa	22	−59	−64	4.29	23
Lobule VIIb (YA n=20 OA n=21)	White Matter	−16	−43	−29	3.93	24
Vermis VIIb (YA n=33 OA n=34)	Brainstem	1	−46	−61	3.79	48
Vermis VIIIb (YA n=33 OA n=35)	Lobule VIIIb	18	−61	−57	3.88	77
	Lobule VI	−13	−78	−24	3.74	39
	Lobule VIIb	8	−74	−50	3.62	15
Vermis IX (YA n=33 OA n=35)	Crus II	44	−41	−45	3.42	10
Vermis X (YA n=33 OA n=35)	Crus II	−26	−85	−44	4.3	90

Table 8

MNI coordinates of the local maxima of brain regions showing greater functional connectivity in older adults than young adults when lobules of the right cerebellar hemisphere were used as seeds

Negative x-values indicate locations in the left hemisphere, while positive x-values indicate locations in the right hemisphere. All results are uncorrected p<.001, with a minimum cluster size of 10 voxels.

Seed	Region	BA	MNI Coordinates			T-Value	Cluster Size
			X	Y	Z		
Lobules I–IV (YA n=33 OA n=35)	Post-Central Gyrus	3	60	−16	46	4.16	12
Lobule V (YA n=33 OA n=35)	Inferior Frontal Gyrus	9	−62	8	26	4.3	11
Lobule VI (YA n=33 OA n=35)	Inferior Frontal Gyrus	9	−62	10	24	4.39	15
Crus I (YA n=30 OA n=34)	Insula	13	−36	−10	22	4.08	14
Crus II (YA n=25 OA n=34)	Lingual Gyrus	18	−14	−82	−4	4.13	11
	Insula	13	34	−34	24	3.74	16
Lobule VIIIa (YA n=19 OA n=22)	Middle Temporal Gyrus	22	−52	−48	−2	4.22	12
Lobule VIIIb (YA n=19 OA n=22)	Inferior Frontal Gyrus	9	−50	2	24	4.16	18
	Post-Central Gyrus	2	−66	−20	28	4.15	10
	Superior Temporal Gyrus	13	46	−18	8	4.34	12
	Middle Temporal Gyrus	37	46	−58	2	4.23	24
	Insula	13	−36	−12	14	3.96	28
			−46	6	8	3.83	11
	Inferior Parietal Lobule	40	−58	−36	40	3.86	42
			58	−24	26	3.7	11
			60	−32	34	3.62	11
Lobule IX (YA n=23 OA n=31)	Superior Temporal Gyrus	13	46	−18	8	4.34	12
	Middle Temporal Gyrus	37	46	−58	2	4.23	24
	Insula	13	−36	−12	14	3.96	28
			−48	6	8	3.83	11
	Inferior Parietal Lobule	40	−58	−36	40	3.86	42
			58	−24	26	3.7	11
			60	−32	34	3.62	11

Seed	Region	BA	MNI Coordinates			T-Value	Cluster Size
			X	Y	Z		
Lobule X (YA n=33 OA n=35)	Superior Temporal Gyrus	22	−48	−36	0	4.79	102
		42	−56	−32	10	3.96	12
	Post-Central Gyrus	3	58	−16	28	4.17	18
	Pre-Central Gyrus	4	28	−20	54	3.39	10
Vermis VIIIa (YA n=33 OA n=35)	Angular Gyrus	39	52	−66	30	4.28	18
	Middle Temporal Gyrus	37	−50	−48	−7	4.03	20
	Inferior Frontal Gyrus	9	−40	6	26	4.01	48
	Middle Frontal Gyrus	46	−48	−34	20	3.98	13
	Anterior Cingulate Cortex	32	−16	10	32	3.89	21
Vermis IX (YA n=33 OA n=35)	Middle Temporal Gyrus	21	60	4	−6	4.15	23
	Anterior Cingulate Cortex	32	−12	38	6	4.07	21
	Precuneus	31	24	−68	18	4.07	12
	Fusiform Gyrus	20	42	−28	−18	3.89	19
	Dorsal Pre-Motor Cortex	6	−44	−16	30	3.79	23
Vermis X (YA n=33 OA n=35)	Inferior Parietal Lobule	40	50	−36	26	3.55	10

Table 9

Correlations with control covariates in older adults

The correlated regions fall within areas that showed greater connectivity in young relative to older adults. Negative x-values indicate regions in the left hemisphere, while positive x-values indicated regions in the right hemisphere. All presented results are thresholded at p<.001, uncorrected and masked with the young greater than older adult contrast network.

Seed Region	Control Variable	Correlated Region	BA	MNI Coordinates			T-Value	Cluster Size
				X	Y	Z		
Lobule V	SNR	Lobule V	--	−6	−64	−10	7.84	15
				6	−62	−8	4.95	13
Lobule VI	SfNR	Posterior Cingulate Cortex	31	8	−48	42	5.45	14
			29	−2	−44	6	4.20	15
		Precuneus	7	0	−52	46	4.43	11
		Lobule VI	--	−30	−56	−22	4.92	29
				28	−58	−18	4.85	43
		Crus I	--	34	−74	−20	3.90	11

Table 10

Correlations between resting state cerebellar networks and sensorimotor and cognitive behavior

Negative and positive x-values indicate regions in the left and right hemispheres, respectively. All presented results are thresholded at p<.001, uncorrected and were masked with the thresholded lobular connectivity networks. Lobules not listed did not exhibit any significant behavioral relationships, or were not analyzed due to sample size (lobules VIIIa and VIIIb)

Seed Region	Behavior	Correlated Region	BA	MNI Coordinates			T-Value	Cluster Size
				X	Y	Z		
Lobules I–IV (n=14)	Working Memory Accuracy	Medial Frontal Gyrus	6	−4	−2	60	5.64	31
Lobule V (n=14)	CV1000 *	Insula	13	34	18	6	5.84	10
	Grooved Pegboard *	Medial Frontal Gyrus	6	4	−20	78	5.12	11
Lobule VI (n=13)	ABC16	Cuneus	19	8	−88	24	5.86	10
Crus II (n=13)	ABC16	Caudate	--	12	18	14	6.76	16
		Thalamus	--	−6	−28	0	6.20	19
	Closed Balance	Posterior Cingulate Cortex	31	4	−40	40	6.27	15
	CV1000 *	Precuneus	31	−8	−56	34	6.52	26
		Supramarginal Gyrus	40	−54	−58	34	5.79	11
	Grooved Pegboard *	Superior Temporal Gyrus	39	46	−54	30	6.33	16
		Precuneus	19	−44	−72	42	5.65	26
		Posterior Cingulate Coretx	31	−6	−52	22	4.56	12
	Working Memory Accuracy	Precuneus	31	−8	−48	36	6.82	16
		Posterior Cingulate Cortex	31	6	−52	22	5.41	36
	Working Memory Reaction Time *	Precuneus	31	4	−52	30	6.06	48
Vermis VI (n=14)	ABC16	Medial Frontal Gyrus	6	4	0	58	5.42	15
Vermis VIIIa (n=14)	CV1000 *	Caudate	--	−20	2	22	4.68	11
	Grooved Pegboard *	Thalamus, Ventral Lateral Nucleus	--	−18	−10	16	6.26	35
		Caudate	--	−20	0	22	6.22	15

* Indicates negative correlations. Lower scores indicate better performance. N indicates the sample size included in each analysis.